Molecular and Functional Study of Monalysin, a Pore-Forming Toxin from Pseudomonas entomophila

Dissertation

Molecular and Functional Study of Monalysin, a Pore-Forming Toxin from *Pseudomonas entomophila*

Graduate School of Medical Sciences

Kanazawa University

Division: Pharmaceutical Sciences

Laboratory: Host Defense and Responses

School Registration No. : 1729012009

Name : Emil Salim

Primary Supervisor Name : Assoc. Prof. Takayuki Kuraishi

ACKNOWLEDGEMENTS

Alhamdulillah, all praise to Allah SWT for giving me the blessing and strength to complete this dissertation.

I would like to express my sincere gratitude to my supervisor Assoc. Prof. Takayuki Kuraishi for giving me an opportunity to study in his Laboratory. Thank to his time, generous guidance, patience and encouragement throughout the whole of my study. I have learned a lot from him about innate immunity, how to perform a good research, many experimental techniques and managing many experiments efficiently. I would like also to thank for his kind support for my family and my career.

Deepest gratitude are also to Prof. Emeritus Yoshinobu Nakanishi, his advice, encouragement and support during his time in this laboratory were really valuable to me. I would like to thank Professor Akiko Shiratsuchi for her kind support and help during her time in this lab, Prof. Ryo Suzuki for his advice during my study. I also would like to acknowledge the former Assist. Prof. Nonaka Saori who trained me many experimental techniques and help me a lot in this lab. My special thanks to the current Assist. Prof. Aki Hori, her advice and support were really essential for me.

I am very grateful to researchers from various institutions, Professor Koki Kamiya (Gunma University), Prof. Takumi Nishiuchi (Kanazawa University), Prof. Shoji Takeuchi (The University of Tokyo), Prof. Noriyuki Kodera (Kanazawa University), in collaboration with us to complete this study.

I would like to extend my gratitude to the alumni and the current members of this lab. Firzan Nainu, PhD, for introducing me to my supervisor and sharing his thoughts and experiences. Rangga Meidianto Asri and Heny Ekowati, PhD, for their kind advice and help. My tutor, Natsumi Yamada for helping me to deal with administration in Japanese both for study and living in this city. Hibiki Kadoguchi for his kindness for picking me with his car during heavy snow. Mayo Kawabata, Andre R. Pratomo, Dini Rahmatika, Koichiro Kawamura, Yuto Kido, Kazuki Fukushima, Min Zhang, Nozoe

Ami, Yoshitaka Furuta, Yuta Amagasa, Mai Sono, Miho Morimatsu, Chin Si, Azusa Kubota, Ikuto Kato, and Kiyoshi Okado for their help and friendship.

I am really grateful to Indonesia Endowment Fund for Education (LPDP) and Ministry of Research, Technology and Higher Education of the Republic of Indonesia for providing me a full financial support via BUDI- LN Scholarship program and the Sasakawa Scientific Research Grant.

My sincere gratitude to my father Syamsul Bahri, my mother Emmy Warni Nasution, my father in law Syahrial Harahap, my brothers, brothers and sisters in law for their continuous support and pray. Special thanks to my beloved wife, dr. Meina Ramadhani Harahap, her pray, endless support, invaluable advice, keep myself motivated to accomplish my study. My thanks also for my sons Salim Al Fatih, Muhammad Hanif, Umar Azka Abdurrahman, and my daughter Farah Kamila, their smiles always light up my life.

Table of Contents

List of Figures and Figure Legends

Abstract

Pseudomonas entomophila is an entomophatogenic bacterium that infects and kills *Drosophila* and other insects upon ingestion. It is a suitable model to study the interaction between pathogen and *Drosophila's* innate immunity. Monalysin, a β-barrel pore-forming toxin from *P. entomophila,* impairs *Drosophila's* tissues leading to the necrotic cell death.

In this study, I present the first purification and characterization of endogenous Monalysin. Monalysin is successfully purified as a pro-from, which is cleaved by trypsin treatment into its active form that is able to kill *Drosophila* cell lines and adult flies. Electrophysiological analysis of Monalysin in a lipid membrane with an on-chip device proves that active Monalysin forms a pore. Using current amplitude for a single pore, this analysis also provides a pore-size estimate of Monalysin and suggests its lipid insertion preferences. Atomic Force Microscope (AFM) analysis in a solution demonstrates that active-Monalysin is stable and composed of an 8-mer complex; which is consistently supported with mass spectrometry data. AFM analysis also proves 8-mer structure of active-Monalysin in a lipid bilayer, and real-time imaging shows dynamic insertion of Monalysin into the lipid membrane. Together, these results suggest that endogenous Monalysin is a pore-forming toxin which has a rigid structure before pore formation in the lipid membrane. This study provides a sophisticated tool to analyze the mechanism of host innate immunity in response to the invasion of entomopathogenic bacteria that produce pore-forming toxin.

Chapter 1 Introduction

Pseudomonas entomophila is an entomopathogenic bacterium, isolated from a single *Drosophila melanogaster* female collected in Calvaire (Guadeloupe) as part of a *Drosophila* bacterial pathogen screen [1]. It is the only *Pseudomonas* species that can naturally infects and kills insects after being ingested. This Gram negative bacterium has become one of the best model to investigate the interaction of insect and microbe. *P. entomophila* was able to cause a systemic immune response in both *Drosophila melanogaster* larvae and adults after ingestion [1]. Oral infection with large doses of this bacterium are particularly pathogenic to *Drosophila* and cause massive disruption of the *Drosophila* gut epithelium. *P. entomophila* was able to kill insects from at least three distinct orders in addition to *Drosophila*, indicating that it has a broad host range and making it a promising model for the study of host-pathogen interactions and the development of bio-control agents for insect pests [2].

Infection with *P. entomophila* induces severe damage in the *Drosophila* gut by generating reactive oxygen species (ROS) generated by host cells and a pore-forming toxin (PFT) released by the bacteria resulting translational inhibition in the intestine and so limits epithelial renewal, which is required to heal the infection's damage [3]. Translational inhibition, is the principal cause of fly mortality since it prevents both immune and repair pathway. As a result, the elimination of bacteria is hampered and the flies' gut becoming shrink and rupture [2].

Monalysin is a secreted PFT of wild type strain *P. entomophila*. Mutation of *pseen3174*, a gene encodes Monalysin, reduce intestinal damage [4]. PFTs are among the most common virulence effectors released by pathogenic bacteria [5]. These proteins form oligomers that can insert to the membrane of target cell leading to the formation of lytic pores. PFTs insertion can be occurred either via the insertion of amphipathic α-helices and β-hairpins. The Monalysin sequence consists of an internal domain containing amphipathic patches flanked by serine and threonine rich sequence, which

is an hallmark of the membrane-spanning region of ß-barrel pore-forming toxins [4]. Monalysin exhibit all the structural features of members of the ß-PFT group [6]. PFTs are produced in immature form to prevent the oligomerization within bacterial cells. Upon release, these proteins are activated by either proteases produced by bacterium itself or enzymes of host digestive tract such as trypsin [4], [6], [7]. Monalysin, is synthesized as a soluble 30.2 kDa pro-toxin, pro-Monalysin. Upon release, pro-Monalysin is activated by proteolytic cleavage at the N-terminus to become 26.5 kDa mature protein [4], [8], [9].

Well-characterized pure Monalysin might be beneficial in studying the interaction between the host and entomopathogenic bacteria that produce damage-inducing toxins. Furthermore, pore-forming proteins such as Monalysin might be employed as biological control agents against insects (e.g., Cry toxin) [10]–[12], as well as biological "nanopores" that are used as single-molecule detectors (e.g., α-hemolysin) [13]. In that sense, utilizing endogenous Monalysin isolated from *P. entomophila* rather than the recombinant protein produced by *E. coli*, which may have a different intracellular environment than *P. entomophila*, might give a more detailed understanding of its protein function. The difference in intracellular environment may result in an altered protein subunit composition, which might affect the structural and functional properties of the toxin. A detailed study of the natural pore-forming protein's structure and dynamics in solution and in the lipid membrane would also provide useful knowledge for a variety of applications. In this study, I successfully purified the native endogenous Monalysin from *P. entomophila* with lethal activity in *Drosophila* cell lines and adult flies. Using electrophysiological data and a high-speed atomic force microscope (HS-AFM), I analyzed its structure and function [14].

Chapter 2 Purification of Endogenous Monalysin from *P. entomophila*

2.1 *P. entomophila* extract as the source of endogenous Monalysin

Kuraishi et al. 2011, previously reported that *P. entomophila* extract prepared by sonication of the bacterial cells with detergent, followed by membrane-filtration caused fly death if ingested [15]. Based on this result, I prompted to examine whether *P. entomophila* extract can be used as a source for purification of endogenous Monalysin. I tested the cytotoxicity effect of the extract on S2 cells which derived from *Drosohila* embryonic hemocytes. I found that almost all cells lost their normal morphology and fell apart after 12 h of incubation (Figure 1). I also performed the CellTiter-Glo assay to measure the viability of the cells. This assay works by measuring ATP level as an indicator of live cells. I found that the cells treated by this extract were dead (Figure 2).

To confirm whether the cytotoxicity of *P. entomophila* extract depends on Monalysin, I tested the cytotoxicity of Monalysin-deficient strain of *P. entomophila* on *Drosophila* S2 cells. I found that the cytotoxicity of the extract from Monalysin-deficient strain of *P. entomophila* was lower compared to that of a wild type (Figure 1 and Figure 2). These results indicate that *P. entomophila* extract contains Monalysin, and could be used as a source for the purification of endogenous Monalysin. Moreover, I used this cytotoxicity assay to find toxic fraction in every purification step.

2.2 Monalysin Purification

Next, I performed Monalysin purification using the strategy displayed in the Figure 3. First, to reduce the total volume of the extract, I precipitated the *P. entomophila* extract or the total lysate using an ammonium sulfate solution and suspended the pellet using a Tris Buffer. Then, the total lysate was fractionated using a column for anion exchange chromatography, and eluted using a linear gradient of 0 to 1 M NaCl. The result indicated that the sub-fractions 4-8 obtained from the anion exchange chromatography were toxic (Figure 4). I precipitated again these active sub-fractions (Fraction III)

using an ammonium sulfate solution and suspended them using a phosphate buffer (Fraction IV). Next, the fraction IV was subjected to a column for gel filtration chromatography, and several sub-fractions were collected. I tested the toxicity of the sub-fractions using the CellTiter-Glo Luminescent Cell Viability Assay and found that only the sub-fraction 1 was toxic. The percentage of recovered activity of this final fraction (Fraction V in Table 1 and Figure 3, sub-fraction 1 in Figure 5) was 6% from the total lysate of *P. entomophila*. Table 1 indicated that the specific activity of this final sub-fraction was increase to 14-fold. I analyzed the chromatogram of the last fraction (Fraction V in Table 1 and Figure 3, sub-fraction 1 in Figure 5) and found a sharp single peak at approximately 460 kDa (Figure 6) and using an SDS-PAGE I observed 30 kDa single band (Figure 7), which is similar with the estimated size of pro-Monalysin monomer. The single band was subjected to mass spectrometric analysis and resulted in specific amino acid sequence of Monalysin (data not shown). Taken together, I concluded that pro-Monalysin, was purified as a homogeneity from the wild type of *P. entomophila*. Note that, the molecular mass of 460 kDa from the gel filtration, which is the multimer of Monalysin, was a little smaller compared to that of found in the previous report [16].

2.3 Activation of pro-Monalysin

In order to be fully active, pro-Monalysin need to be cleaved by protease AprA released by *P. entomophila* [16]. Trypsin was reported to recapitulate the activity of AprA in the cleavage of recombinant pro-Monalysin [16]. Thus, I used trypsin to examine if my endogenous Monalysin is converted from a pro-form into an active-form. In line with the previous report [16], the SDS-PAGE analysis indicated that 30 kDa pro-Monalysin was transformed into 27 kDa active-Monalysin (Figure 8). Henceforward, trypsin-treated Monalysin is referred as “active-Monalysin” since its cytotoxicity was significantly higher compared to that of pro-Monalysin (Figure 9).

To rule out that this cytotoxicity may be derived from trypsin, I treated *Drosophila* S2 cells with trypsin. The result indicated that trypsin do not have cytotoxicity activity (Figure 9). Moreover, I

found that the activity of pro-Monalysin and active-Monalysin were dose-dependent manner (Figure 10). The estimation of lethal concentrations 50% (LC_{50}) of pro- and active-Monalysin from the Figure 10 were 1.4 and 3.1 μg/mL, respectively (Figure 11). This result indicated that pro-Monalysin also toxic. The toxicity of pro-Monalysin without trypsin treatment may be not due to its ability to form pore, since the efficiency of pro-Monalysin to form pore is much lower compared to that of active-Monalysin in artificial membrane (Figure A. 2). The possible cause is may be the proteases in the S2 cell in a culture medium or on the cell surface performed proteolytic cleavage to activate pro-Monalysin.

The cell death caused by active-Monalysin was occurred via necrosis not apoptosis. The result showed that active-Monalysin did not stimulate 3/7 caspase activity, while cycloheximide (reported to induce apoptosis in S2 cells) displayed strong induction of the caspase 3/7 (Figure 12, [17]).

2.4 Toxicity of active-Monalysin In Vivo

To confirm if the endogenous Monalysin had toxic effect activity in vivo, I injected the toxin into adult hemolymphs. Active-monalysin killed adult flies more significantly compared to that of pro-Monalysin and degraded-Monalysin which was subjected to trypsin digestion for a long time to be completely degraded (Figure 13). Furthermore, active-Monalysin displayed a dose-dependent toxicity on fly survival (Figure 14).

Next, I also determined the toxicity of active-Monalysin on the gut of adult fly by feeding orally *dcy* mutant with active-Monalysin. I used *dcy* mutant because the previous study reported that this mutant was susceptible to *P. entomophila* extract infection fed orally [15]. The result showed that the number of mitotic stem cells was increase as indicated by the increase of phospho-histone H3 (PH3), the marker of gut repair after damage (Figure 15). Additionally, I performed immunostaining of Discs large (Dlg), the marker of septate junction and also nuclear staining in flies following the injection of active-Monalysin. Figure 16 showed that the organization of the epithelial cells was

damage indicating that flies intestine could be damaged by Monalysin. Taken together, these results suggest that the purified Monalysin is toxic in vivo.

2.5 Induction of active-Monalysin on the expression of antimicrobial peptides (AMP) and stress gene

I also tested if Monalysin injection could stimulate the expression of antimicrobial peptides (AMP) and stress gene in adult flies, as tissue damage could induce infection-independent humoral innate immunity. Real-time quantitative PCR (RT-qPCR) analysis indicated that the expression of *Drosomycin (Drs)*, a read-out of the activation of the Toll pathway, was increase significantly (Figure 17). Furthermore, the result also showed that the expression of *Turandot A (TotA)*, a read-out of the JAK-STAT pathway activation, was also increase significantly (Figure 18). These data suggest that Monalysin activate the innate immune and stress pathway, perhaps through the induction of the Toll and/or JAK-STAT pathways. However, Monalysin did not stimulate *Diptericin* (*Dpt*) and *puckered* (*puc*) gene expression, a read-out indicating the activation the IMD pathway and Jun-N-terminal kinase (JNK) pathway, respectively (Figure 19 and Figure 20). *P. entomophila* cannot be recognized by the Toll pathway since this Gram-negative bacterium does not possess the Lys-type peptidoglycan. In addition, the results showed that degraded-Monalysin did not activate the expression of *Drs* and *TotA* (Figure 17 and Figure 18). Peptidoglycan-contamination test using Silkworm Larvae Plasma (SLP) did not indicate that active-Monalysin was contaminated with peptidoglycans, the ligand that activate innate immunity (Figure 21). These results might rule out the probability that active-Monalysin might be contaminated by some PAMPs that normally activate humoral immunity. Additionally, the results suggest that the tissue damage in adult *Drosophila* caused by Monalysin might provoke a humoral innate immune response and stress response. Collectively, these results indicate that I successfully performed the purification of endogenous Monalysin, with toxic and damage-inducing activity in *Drosophila*.

Chapter 3 Discussion

In this study, for the first time, I successfully purified the endogenous Monalysin derived from *P. entomophila*. Using electrophysiological analysis, I confirmed that this pro-form is activated by trypsin. The cytotoxic activity of active-Monalysin on *Drosophila* cell line and adult flies were also confirmed. Particularly, HS-AFM analysis on the structure and dynamics of Monalysin in solution and within the lipid membrane, revealed that the active-octamer structure is stable. This study suggests that endogenous Monalysin appears to be one of the best model toxins produced by entomopathogenic bacteria. In addition, the information derived from electrophysiological analysis about the pore size is important to develop this endogenous toxin as a biological nanopore.

I performed pro-Monalysin purification based on cytotoxic activity from cell pellets of *P. entomophila* suggesting that a vast amount of pro-form is stored inside the cells. HS-AFM analysis indicated that pro-Monalysin and active-Monalysin diameters are estimated to be around 11 nm and their heights are approximately 14 and 5–7 nm, respectively. Both dimensions are too big to be released by the secretion system of *P. entomophila*. This bacterium has type I and II secretion systems with secretion pore diameters that are generally less than 5 nm [18]–[20]. However, autolysis can be occurred in *P. entomophila*, particularly over 30^{o}C. *P. entomophila* may be lysed in the host's intestine leading to the release of pro-Monalysin which subsequently cleaved by proteases produced by bacteria such as AprA or proteases generated by the host resulting the transformation of the pro-form to become the active-form. At high concentration, pro-Monalysin forms the trimer complex in the PBS buffer resulting the cleavage site might be hidden thus preventing the activation by proteolytic enzyme to become an active-form in *P. entomophila*. The investigation of localization in subcellular compartment and estimated concentration of pro-Monalysin in *P. entomophila* should be performed in the future study.

The most well-characterized PFT is probably Cry toxin, generated by the Gram-positive bacterium *Bacillus thuringiensis*, which induces tissue damage in insect. This toxin, commonly used

as a biological pesticide, is one of the member of a large family that consist of more than 350 toxins which share similar characteristics [16]. Upon ingestion, this toxin is cleaved by intestinal proteases to become active. The active-Cry toxin is considered a monomer molecule, bind to a receptor on the midgut epithelial cell membrane inducing cell lysis and tissue damage [16], [21]. However, my study revealed that endogenous Monalysin was composed of a pore-forming multimer from the initial state and shows that their insertion into the lipid membrane is receptor-independent. Importantly, since Cry toxin target is specific insect species through selective toxin-receptor binding, one needs to use a genetic trick when applying them on flies, e.g., overexpression of the Cry1Aa receptor and the use of Cry1Aa thereafter [21]. Therefore, if one need to induce tissue damage in a non-specific manner, Monalysin injection or ingestion would be a simple method. As indicated in our study, injection of endogenous Monalysin, through a standard procedure, effectively killed adult flies and stimulated the response of innate immunity. The theoretical knowledge derived from our study enable the application of this toxin as a sophisticated tool to investigate innate immunity that induced by injury in the context of microbial infections. Since the endogenous Monalysin can be obtained milligram order from 1 L of bacterial culture, this toxin can be used in the various of experiment.

Real-time dynamics of Monalysin in action was revealed from HS-AFM analysis (Figure A. 16). The structure of pro-Monalysin purified from *P. entomophila* was 16-mer complex, however, recombinant Monalysin from *E. coli* showed 18-mer structure. This difference may be due to different techniques or hosts used in the expression of Monalysin. The tendency of pore-forming toxins to form different subunit stoichiometry in solution than in crystal, may also contribute to this discrepancy. For instance, X-ray crystallography showed that α-hemolysin form heptamer structure, in contrast to AFM analysis showed that this toxin showed hexamer structure [21]. Together, this report and my study suggest that pore-forming toxins may form two different stable structures depend on their conditions. The investigation on the crystal structure of endogenous Monalysin should be performed in the next study.

Active-Monalysin generated by trypsin treatment has an 8-mer composition and approximately halves in height, suggesting that pro-Monalysin is half dissociated into an 8-mer pair well before insertion. It attaches and forms pores in the lipid bilayer without profound structural change. Note that, Monalysin was preferentially inserted into the edge of the lipid membrane, indicating that Monalysin could recognize the curvature of target membrane. Eukaryotic cell membrane have some of high curved regions such as the part of endocytosis and exocytosis and the edge of filopodia. These regions play important roles for cell signaling, intracellular communication, and cell movement [21]. Particularly, when immune system is activated, macrophages extend a lot of filopodia. These cells and/or other membrane biological membrane parts might be the targets of Monalysin or its relatives. In addition, the microvilli tip of the *Drosophila*'s enterocytes might be the entry point for Monalysin insertion [4].

Furthermore, Monalysin inserts itself generally within lipid bilayers with high ratio of PC as indicated from the electrophysiological analysis. The chemical nature of lipids determines how they bundle side-by-side in a monolayer and thus affects the curvature of the monolayer. PC, for example, forms nearly flat monolayers; lysophospholipids, form positively curved monolayers; and DOPE forms negatively curved monolayers [22]. Notably, some membrane phospholipids are metabolized into eicosanoids and lysophospholipids when the cell is activated [22]. Highly curved portions which are rich of lysophospholipids during cell signaling might be the area at which active-Monalysin insertion occurs. According to this point of view, active-Monalysin could target not only local membrane subdomains, but also specific cell types and/or cell activation status. These features may then specify host and position where Monalysin is toxic. In vitro and in vivo studies need to be carried out to investigate more specific lipid preferences and the optimal radius of curvature for Monalysin insertion. Further research to reveal the accurate mechanism of action of active-Monalysin during pore formation is needed.

Materials and Methods

Bacteria Stocks, Other Materials, and Cell Culture

P. entomophila wild-type strain L48 and a Monalysin mutant *mnl* were kindly given by Dr. B. Lemaitre. S2 cells from *Drosophila* hemocytes were cultured in Schneider's *Drosophila* medium (Thermo Fisher SCIENTIFIC) containing 10% (v/v) heat-inactivated FBS, 100 units/mL penicillin, and 100 g/mL streptomycin.

Purification of Pro-Monalysin

P. entomophila was grown in LB at 29°C overnight and collected by centrifugation at 8,700 × g at 4°C for 15 min. The cell pellets were washed with PBS and lysed in PBS containing 2% (w/v) CHAPS. Cells were sonicated overnight at 4°C, then filtered through a 70 μm Cell Strainer (BD Falcon) and centrifuged at 9,000 g for 20 min at 4°C to eliminate insoluble pellets. The supernatant was diluted 10 times with PBS, filtered through a 0.22 μm filter (Corning), and dialyzed with PBS for 9 h to exchange the solvent. Total lysate (*P. entomophila* extracts) was precipitate with ammonium sulfate (25–50%). To eliminate salts, the pellet was dissolved in 20 mM Tris-HCl, pH8.0, and dialyzed against the same buffer for 9 h. The dialysate was then subjected to anion exchange chromatography using a HiTrap Q HP column (GE Healthcare), which was pre-equilibrated in 20 mM Tris-HCl, pH8.0, and eluted with a linear gradient of 0 to 1 M NaCl dissolved in 20 mM Tris-HCl, pH8.0 at a flow rate of 1 mL/min for 30 min. Following a cell viability assay, the cytotoxic fractions were collected and concentrated using ammonium precipitation (50%). The pellet was dissolved in a 10 mM sodium phosphate buffer, pH 7.4, containing 140 mM NaCl, and then subjected to gel filtration chromatography with a Superdex 200 Increase 10/300 GL column (GE Healthcare), pre-equilibrated and eluted with the same buffer at a flow rate of 0.75 mL/min.

SDS-PAGE was used to assess the peak eluted at 13-14 min (molecular weight about 460 kDa). To ensure purity, the gel was stained with Coomassie Brilliant Blue (Kanto Chemical Co., Inc.). The

30 kDa band was excised and subjected to mass spectrometry analysis. The protein concentrations of fractions were determined using the Lowry method with Bio-Rad DC protein assay kit (Bio-Rad). To obtain active-Monalysin, trypsin-treatment at 0.2 mg/mL was applied to purified pro-Monalysin (175 μg) and incubated at 25°C for 10 min, followed by the addition of a Protease Inhibitor Cocktail for General Use (nacalai tesque, Cat# 04080-11). To fully degrade Monalysin, 0.2 mg/mL trypsin was applied to pro-Monalysin (10 μg) and incubated at 37°C for 58 h.

Mass Spectrometry

To identify the protein in the cytotoxic fraction, MALDI-TOF MS/MS analysis was conducted at the Institute for Gene Research, Advanced Science Research Center, Kanazawa University, using a tandem mass spectrometer (4,800 plus MALDI TOF/TOF^{TM} Analyzer [Sciex]) with 2,5-dihydroxybenzoic acid (DHB) as a matrix as described in Asano and Nishiuchi [23]. In brief, a cytotoxic fraction was loaded onto an SDS-acrylamide gel, and a 30 kDa band was excised and in-gel digested with trypsin. MALDI-TOF/TOF was used to analyse the digested peptides. The data was subjected to the Protein Pilot ver.4.0 (Sciex) against the *Pseudomonas entomophila* (NCBI, Tax ID 312306) protein database (2017-8-23).

To examine the molecular weight of the active-Monalysin multimer, MALDI-TOF analysis was conducted using the UltrafleXtreme MALDI TOF/TOF Analyzer (Bruker Daltonix) at Fukui Prefectural University using sinapic acid (SA) as a matrix. First, areas on the MALDI plates were coated with the SA solution. The mixture of active-Monalysin and SA solution was dropped onto the SA-coated spots. To obtain the molecular weight, each spot was analyzed by MALDI-TOF (ultrafleXtreme). The results from several measurements were combined via analysis software version 4.1.2.

Cell Viability Assay

S2 cells (1.5-8.0×10^5 cells in 100 µL) were cultured in a 96-well plate. 10 µL of *P. entomophila* extract or collected fractions after chromatography, purified pro-Monalysin (1.5 µg/mL), active-Monalysin (1.5 µg/mL), or trypsin (3.8 × 10^{-2} µg/mL) were added and incubated at 25°C for 12-18 h. Cell viability was measured by luminescence from a CellTiter-Glo Luminescent Cell Viability Assay (Promega) with a Spark 10M (TECAN). Cell viability is expressed as a relative value, with luminescence in cells incubated with the buffer (negative control) equal to 100%. To determine total activity, cell viability after incubation with serial diluted fractions was measured and total activity was calculated as 1 unit corresponding to activity that yields 70% cell viability. Specific activity was expressed as total activity divided by total protein (mg).

Caspase-3/7 Activity Assay

S2 cells (1.5 × 10^5 cells in 100 µL) were cultured onto a 96-well plate. Cycloheximide and active-Monalysin were added at 1.5 µg/mL and incubated at 25°C for 6, 12, 18, and 24 h. Caspase-3/7 activity was measured by luminescence from a Caspase-Glo 3/7 Assay (Promega) using a Synergy HTX (BioTek).

Monalysin Injection and Survival Assay

Oregon R *Drosophila melanogaster* (females, 3-7 days after eclosion) were injected with a pro-Monalysin, active-Monalysin, or degraded-Monalysin solution (1 mg/mL) into their hemolymph by micro-injection (70 nL per fly), and kept at 25°C. One hour after injection, surviving flies were counted. To determine dose-dependent activity, flies were injected with active-Monalysin solution (3-30 µg/mL), and surviving flies were counted every 12 h for 60 h.

Total RNA Extraction and Real-Time PCR

Oregon R *Drosophila melanogaster* (females, 3-7 days after eclosion) were injected with an active-Monalysin, degraded-Monalysin solution (50 μg/mL), or 1,000 times dilution of heat-killed *E. coli* into their hemolymph and kept at 25°C for 3, 6, 20 h. The heat-killed *E. coli* was obtained from overnight culture of *E. coli* (DH5α) without dilution, heated at 100°C for 30 min, sonicated for 10 min, and then diluted with water. To measure the *Drosomycin* (*Drs*), total RNA of the collected flies was extracted with Sepasol-RNA I Super G (nacalai tesque) and subsequently used for cDNA synthesis with ReverTra Ace reverse transcriptase (TOYOBO) and oligo (dT)12-18 primers. To quantify the *Diptericin* (*Dpt*), *puckered* (*puc*), and *Turandot A (TotA*), isolated RNA were subjected to DNase treatment (Promega, M6101), followed by cDNA synthesis with ReverTra Ace reverse transcriptase (TOYOBO) and oligo (dT)12-18 primers. Quantitative real-time PCR (RT-qPCR) was conducted using a LightCycler 480 (Roche Diagnostics). *rpL32* was used as an internal control. The following primers were used for RT-qPCR: *Drs* forward, TTGTTCGCCCTCTTCGCTGTCCT; *Drs* reverse, GCATCCTTCGCACCAGCACTTCA; *Dpt* forward, GTTCACCATTGCCGTCGCCTTAC; *Dpt* reverse, CCCAAGTGCTGTCCATATCCTCC; *puc* forward, GGCCTACAAGCTGGTGAAAG; *puc* reverse, AGTTCAGATTGGGCGAGATG; *TotA* forward, CCAAAATGAATTCTTCAACTGCT; *TotA* reverse, GAATAGCCCATGCATAGAGGAC; *rpL32* forward, AGATCGTGAAGAAGCGCACCAAG; *rpL32* reverse, CACCAG GAACTTCTTGAATCCGG.

Immunohistochemistry

For oral ingestion of Monalysin, *dcy1* flies (Bloomington #26106, females, 3-7 days after eclosion) obtained from the Bloomington *Drosophila* Stock Center were starved for 2 h at 29°C, then placed in a fly vial containing the food solution. The food solution was prepared by mixing active-Monalysin solution (4 mg/mL) and 5 % sucrose (1:1), which was added to a filter disk that entirely covered the surface of the standard fly medium. Flies were placed at 29°C for 8 h, then their guts were

dissected out. Antibody staining was carried out as previously described by Kenmoku et al. [24] using 1:200 rabbit anti-PH3 (Cell Signaling, Cat #9701), 1:50 mouse anti-Dlg (Developmental Studies Hybridoma Bank), and 1:200 Alexa 555-coupled and Alexa 488-coupled secondary antibodies (Thermo Fisher SCIENTIFIC). Nuclei were stained with 0.1 μg/mL of 4',6-diamidino-2-phenylindole (DAPI). Samples were visualized using a LSM710 confocal microscope (Carl Zeiss) or observed by a conventional fluorescent microscope and images were reconstructed by Photoshop (Adobe).

SLP Assay for Purified Monalysin

To determine the contamination level of peptidoglycan, 10 μL of 0.001-1 mg/mL pro-Monalysin, active-Monalysin and degraded Monalyin were incubated with 40 μL of Silkworm Larvae Plasma (SLP) reagent (Wako) at 25°C for 30 min in a 96-well plate. The SLP reagent contains all components of the prophenoloxidase cascade system triggered by peptidoglycans resulting the activation of prophenoloxidase. The activated prophenoloxidase then oxidizes 3,4-dihydroxyphenylalanine (DOPA) in the substrate, resulting the formation of black melanin pigment. The amount of peptidoglycan was visually determined as the blackness of the mixture. The same test was performed on multiple dilutions (1/10, $1/10^2$, $1/10^3$, $1/10^4$) of heat-killed *E. coli* solution as a positive control.

Figures and Figure Legends

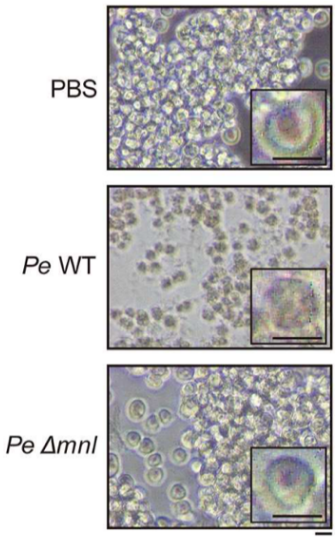

Figure 1. Phase contrast images of S2 cells after incubation with PBS, and *P. entomophila* extracts from wild type (*Pe* WT) or Monalysin-deficient strain (*Pe* Δ*mnl*).
P. entomophila extracts containing 15 µg protein was added to 100 µL of 8×10^5 cells. Incubation time was 12 h. The square on the bottom right side shows magnification images with 20 µm scale bar. Due to cell debris, the area around S2 cells incubated with *Pe* WT extracts appears to be whiter than the rest.

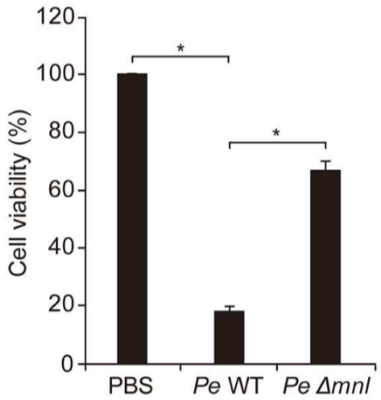

Figure 2. Cell viability of S2 cells incubated with PBS, *Pe* WT or *Pe* Δ*mnl*.
Cell viability was determined using a CellTiter-Glo Luminescent Cell Viability Assay. S2 cells were incubated with *Pe* WT or *Pe* Δ*mnl* total lysates (15 μg protein/8 × 10^5 cells in 100 μL) for 12 h. Cell viability is shown relative to luminescence in cells incubated with PBS, taken as 100%. The data are presented as means ± S.E. from triplicate samples (*$P < 0.05$, as calculated by a Student's t-test).

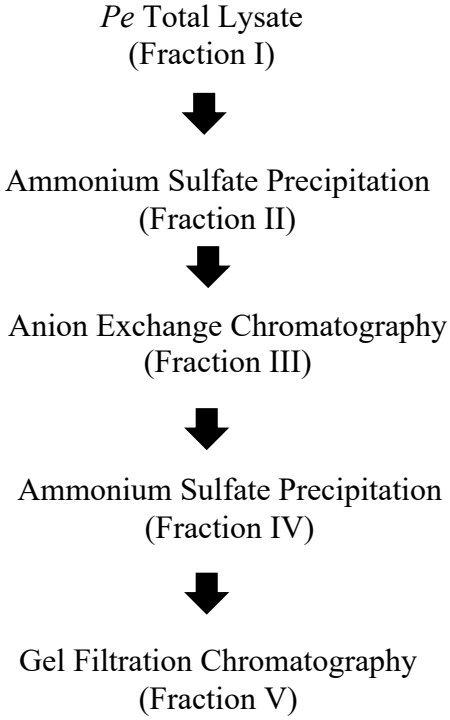

Figure 3. Purification Step of Endogenous Monalysin

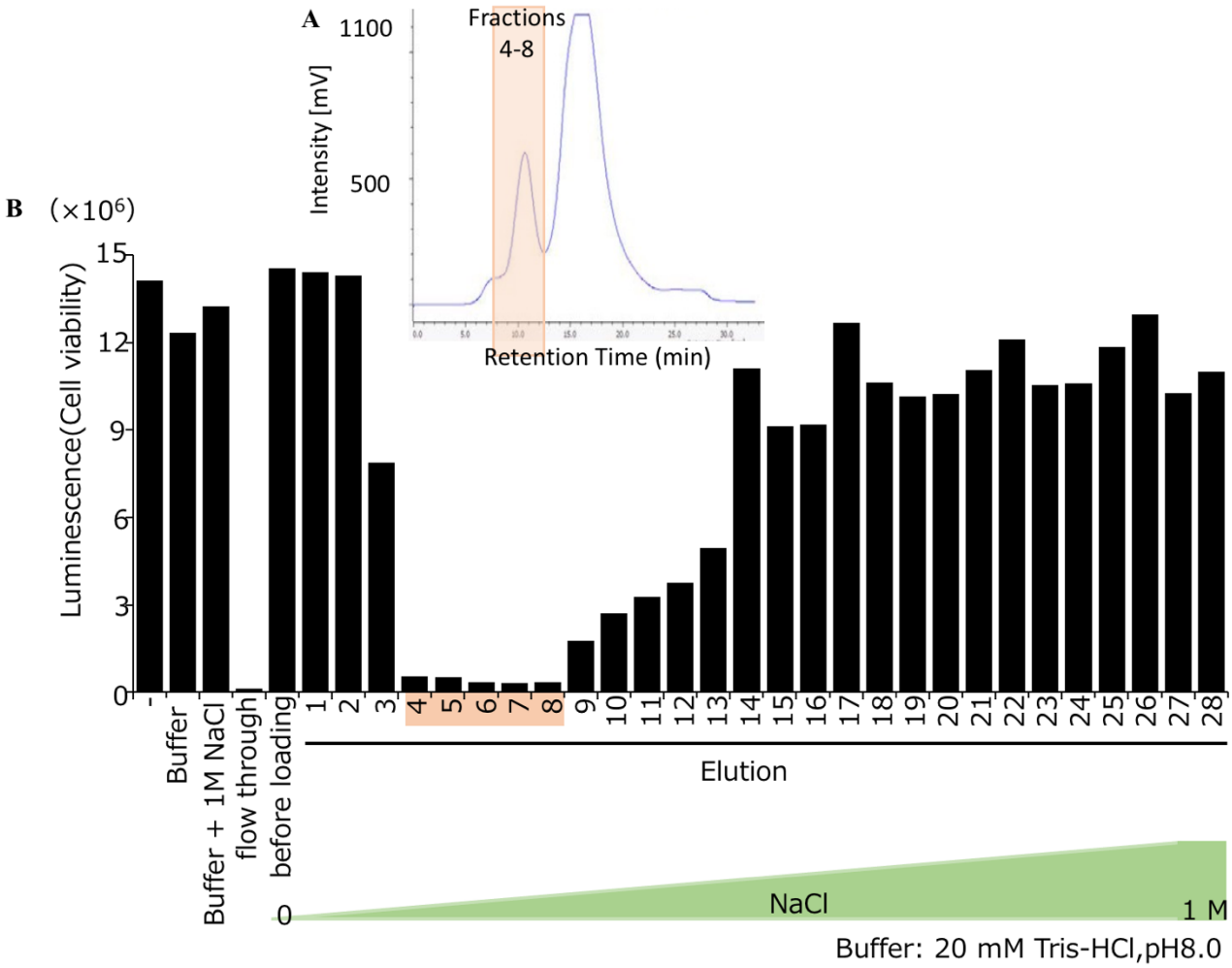

Figure 4. Cytotoxic activity of sub-fractions obtained from anion exchange chromatography.
A. Chromatogram of anion exchange chromatography using a HiTrap Q HP column, which was pre-equilibrated in 20 mM Tris-HCl, pH8.0, and eluted with a linear gradient of 0 to 1 M NaCl dissolved in 20 mM Tris-HCl, pH8.0 at a flow rate of 1 mL/min for 30 min. **B.** Cell viability assay of sub-fractions from anion exchange chromatography. Cell viability was determined using a CellTiter-Glo Luminescent Cell Viability Assay. S2 cells were incubated with the sub-fractions for 12 h. Cell viability is shown as luminescence.

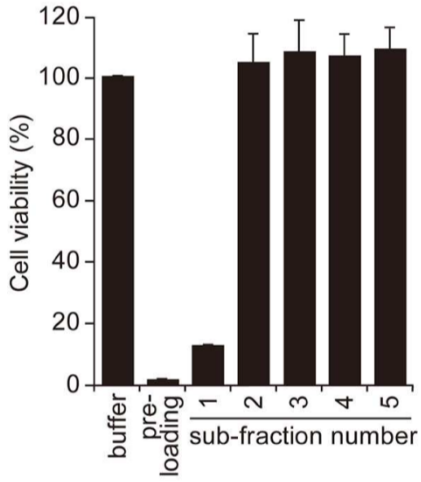

Figure 5. Cytotoxic activity of sub-fractions obtained from gel filtration chromatography.
Cell viability was determined using a CellTiter-Glo Luminescent Cell Viability Assay. S2 cells were incubated with sub-fractions for 12 h. Cell viability is shown relative to luminescence in cells incubated with PBS, taken as 100%.

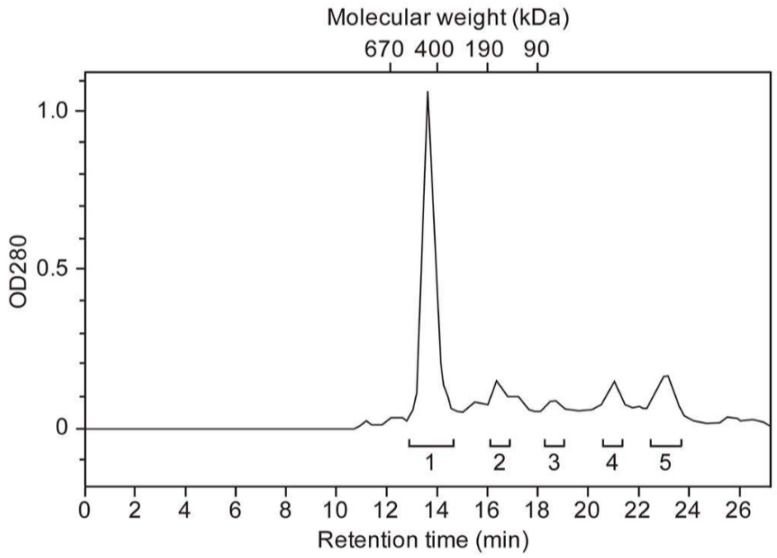

Figure 6. Chromatogram of gel filtration chromatography.
Gel filtration chromatography was performed using a Superdex 200 Increase 10/300 GL column (GE Healthcare), pre-equilibration and elution was performed using 10 mM sodium phosphate buffer, pH 7.4, containing 140 mM NaCl at a flow rate of 0.75 mL/min.

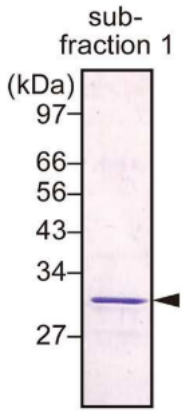

Figure 7. SDS-PAGE analysis of sub-fraction 1.
Coomassie Brilliant Blue was used for the gel staining. The arrowhead shows a 30 kDa pro-Monalysin monomer. The numbers on the left side indicate molecular weight.

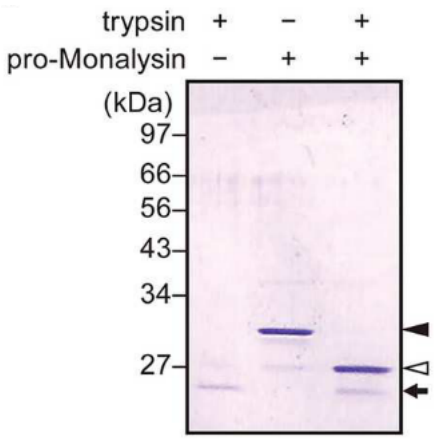

Figure 8. An SDS-PAGE analysis of purified pro-Monalysin before and after trypsin treatment. Coomassie Brilliant Blue was used for the gel staining. Trypsin was incubated with purified pro-Monalysin (0.2 mg/mL) for 10 min. Closed and open arrowheads denote a 30 kDa pro-Monalysin monomer and a 27 kDa active-Monalysin monomer, respectively. The arrow indicates trypsin.

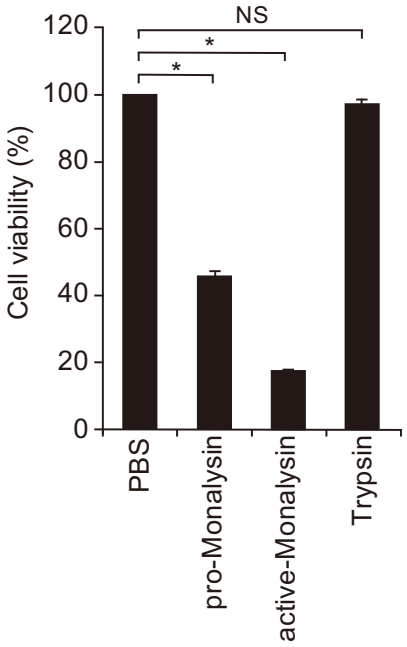

Figure 9. Cell viability after incubation with pro-Monalysin, active-Monalysin, and trypsin.
S2 cells (1.5×10^6 cells in 100 µL) were incubated with of pro-Monalysin (1.5 µg/mL), active-Monalysin (1.5 µg/mL) and trypsin (0.04 µg/mL, expected amount included in active-Monalysin solution) for 18 h. CellTiter-Glo Luminescent Cell Viability Assay was used to measure cell viability. Cell viability is shown, relative to luminescence in cells incubated with PBS, taken as 100%. The data are presented as means ± S.E. from triplicate samples in two independent experiments. (*$P < 0.05$; NS, not significant, as calculated by a Student's *t*-test).

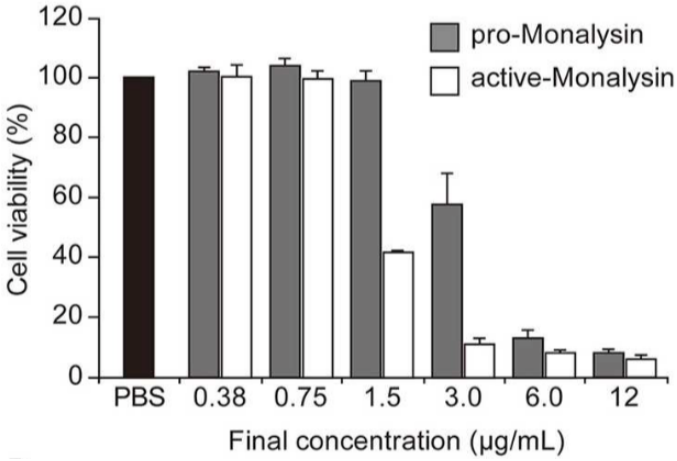

Figure 10. Cell viability after incubation with pro-Monalysin and active-Monalysin.
S2 cells (1.5×10^5 cells in 100 μL) were incubated with the various concentrations of pro-Monalysin or active-Monalysin for 18 h. CellTiter-Glo Luminescent Cell Viability Assay was used to determine cell viability. Cell viability is shown, relative to luminescence in cells incubated with PBS, taken as 100%.

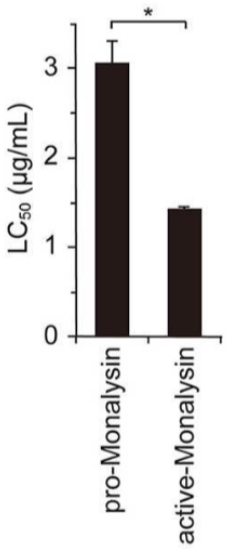

Figure 11. LC_{50} of pro-Monalysin and active-Monalysin.
LC_{50} was estimated from data in the Figure 10. The data are presented as means ± S.E. from triplicate samples (*$P < 0.05$, as calculated by a Student's t-test).

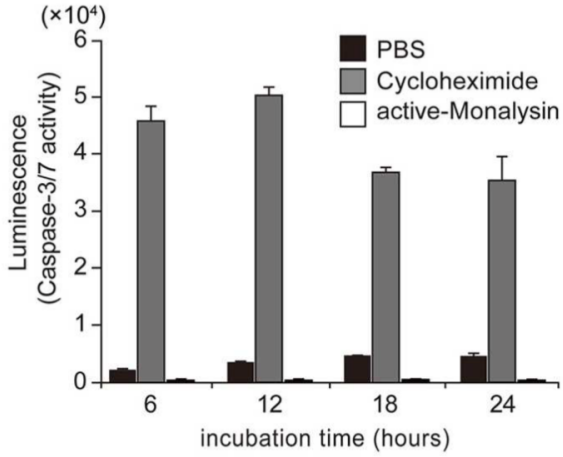

Figure 12. Caspase-3/7 activity in cells after incubation with active-Monalysin.
S2 cells (1.5×10^5 cell in 100 µL) were incubated with active-Monalysin or Cycloheximide (to induce apoptosis) at 1.5 µg/mL for 6, 12, 18 and 24 h. Caspase-3/7 activity was determined as luminescence using a Caspase-Glo 3/7 Assay. The data are presented as means ± S.E. from duplicate samples in two independent experiments.

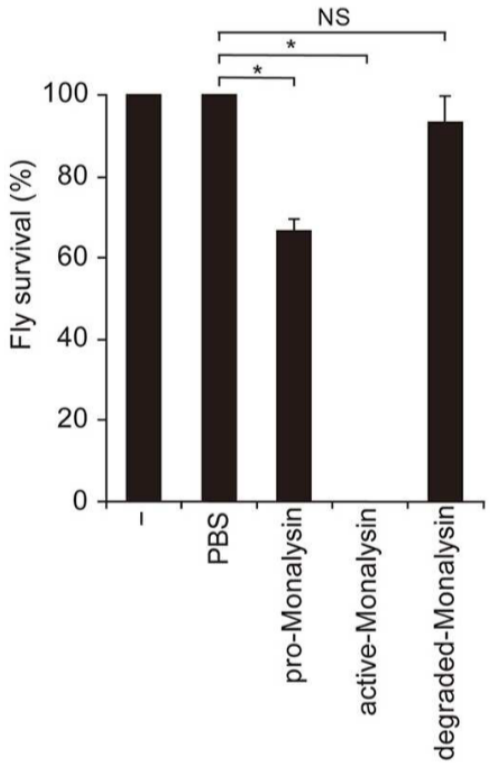

Figure 13. Survival analysis of adult flies after injection with pro-Monalysin, active-Monalysin, or degraded-Monalysin.

Pro-Monalysin, active-Monalysin, or degraded-Monalysin 1 mg/mL was injected into flies hemolymph, and flies survival were monitored after 1 h (*$P < 0.05$; NS, not significant, as calculated by a Student's t-test). The minus indicates un-injected flies. The data are presented as means ± S.E. from three vials (10 flies/each) of two independent experiments.

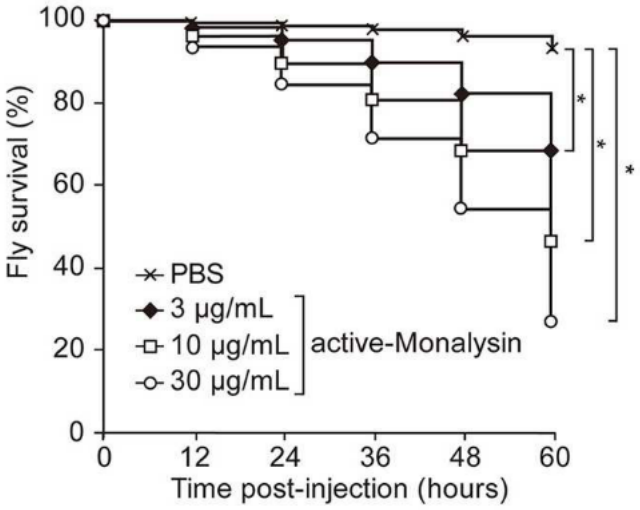

Figure 14. Survival analysis of adult flies upon injection with active-Monalysin.
Flies were injected with active-Monalysin 3-30µg/mL, then, the flies survival were observed at 12, 24, 36, 48, and 60 h after injection. (*$P < 0.0001$, as calculated by a log-rank test).

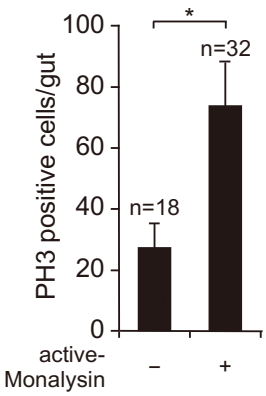

Figure 15. Quantification of PH3-positive cells per gut in *dcy*^{1} flies at 8 h after oral ingestion of 2 mg/mL of active-Monalysin.
(−) indicates sucrose feeding, and (+) indicates active-Monalysin feeding. 18 and 32 guts were observed in flies of (−) or (+) oral ingestion, respectively.

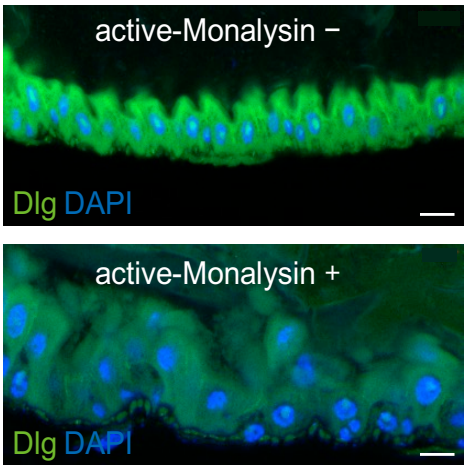

Figure 16. The confocal microscopy images of posterior midgut in *dcy*^{1} flies without (−) or with (+) oral injection of active-Monalysin.
The septate junction marker Dlg (green) and nucleus (blue) were visualized by anti-Dlg antibodies and DAPI, respectively. Scale bar; 10 μm.

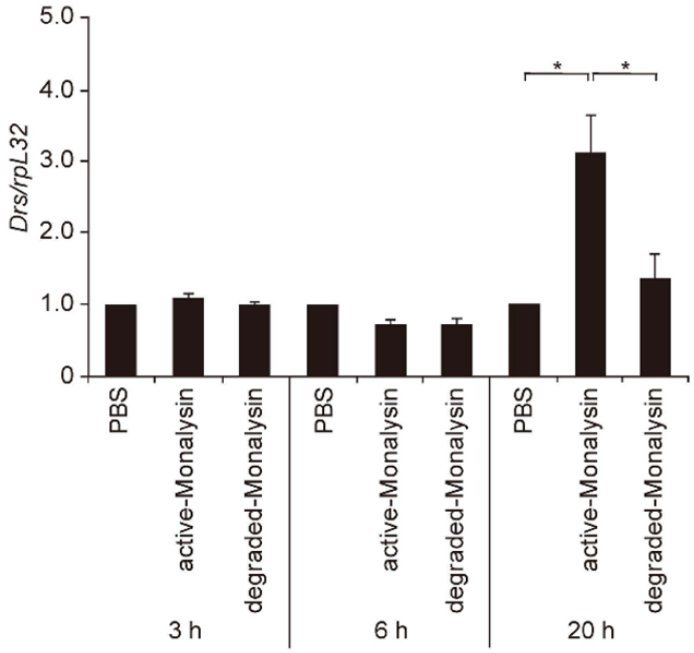

Figure 17. *Drosomycin* (*Drs*) expression in adult flies after injection of Monalysin
Real-time qPCR analysis of *Drs* expression in adult flies at 3, 6, 20 h after an injection of PBS, 50 μg/mL active-Monalysin, or degraded-Monalysin; *rpL32* was used as an internal control. The data is shown, relative to value in PBS-injected flies at each time point, taken as 1.0. The means ± S.E. obtained from 4-6 samples (one sample is derived from 10 flies) are presented. Data are representative of two independent experiments (*$P < 0.0001$, as determined by a Student's *t*-test).

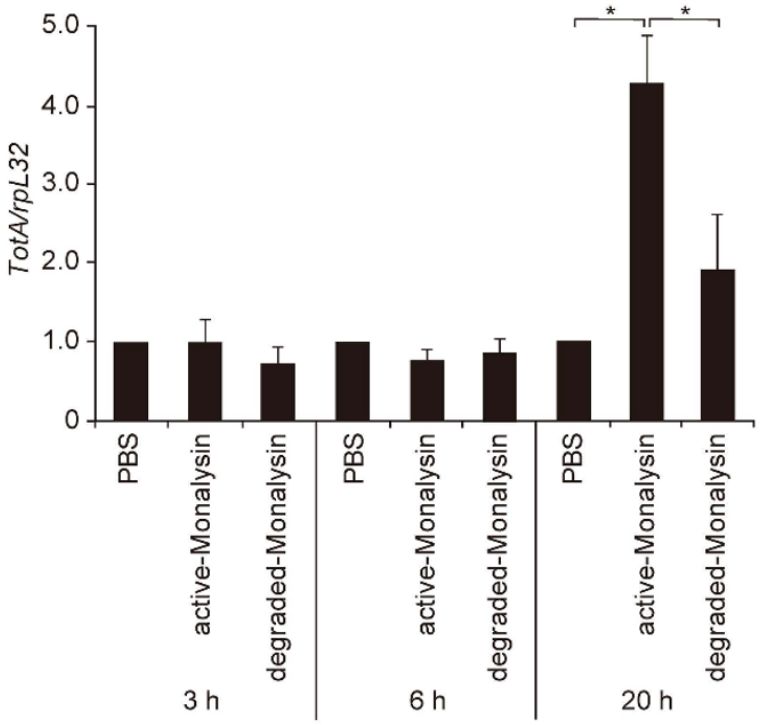

Figure 18. *Turandot A* (*TotA*) expression in adult flies after injection of Monalysin.
Real-time qPCR analysis of *TotA* expression in adult flies at 3, 6, 20 h after an injection of PBS, 50 μg/mL active-Monalysin, or degraded-Monalysin; *rpL32* was used as an internal control. The data is shown, relative to value in PBS-injected flies at each time point, taken as 1.0. The means ± S.E. obtained from 4-6 samples (one sample is derived from 10 flies) are presented. Data are representative of two independent experiments (*$P < 0.0001$, as determined by a Student's *t*-test).

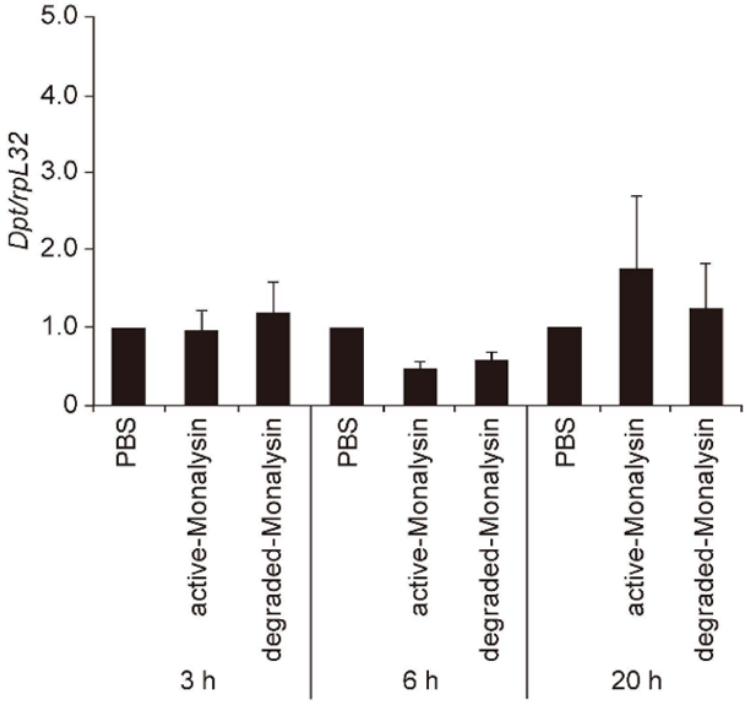

Figure 19. *Diptericin* (*Dpt*) expression in adult flies after injection of Monalysin.
Real-time qPCR analysis of *Dpt* expression in adult flies at 3, 6, 20 h after an injection of PBS, 50 μg/mL active-Monalysin, or degraded-Monalysin; *rpL32* was used as an internal control. The data is shown, relative to value in PBS-injected flies at each time point, taken as 1.0. The means ± S.E. obtained from 4-6 samples (one sample is derived from 10 flies) are presented. Data are representative of two independent experiments (*$P < 0.0001$, as determined by a Student's *t*-test).

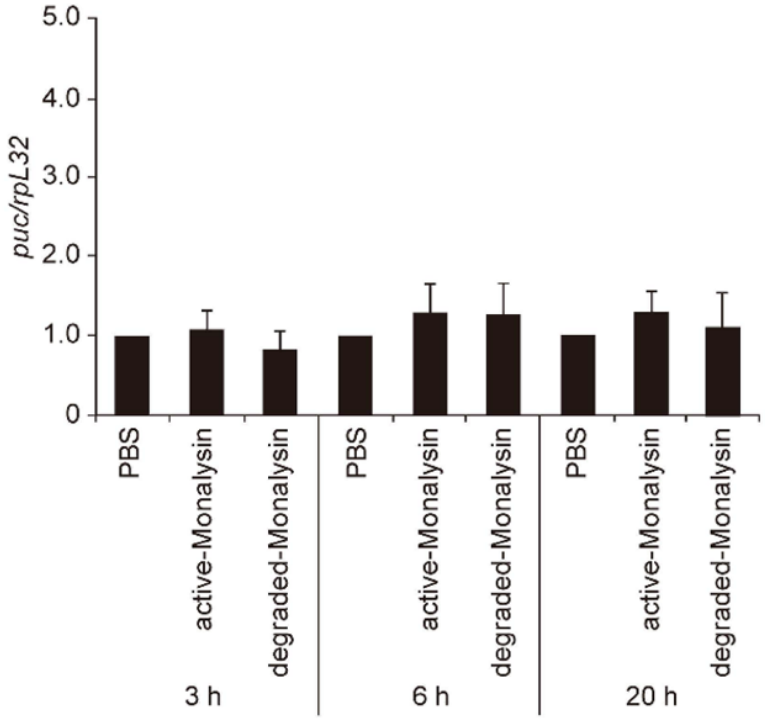

Figure 20. *puckered* (*puc*) expression in adult flies after injection of Monalysin.
Real-time qPCR analysis of *puc* expression in adult flies at 3, 6, 20 h after an injection of PBS, 50 μg/mL active-Monalysin, or degraded-Monalysin; *rpL32* was used as an internal control. The data is shown, relative to value in PBS-injected flies at each time point, taken as 1.0. The means ± S.E. obtained with the data from 4-6 samples (one sample is derived from 10 flies) are presented. Data are representative of two independent experiments (*$P < 0.0001$, as determined by a Student's *t*-test).

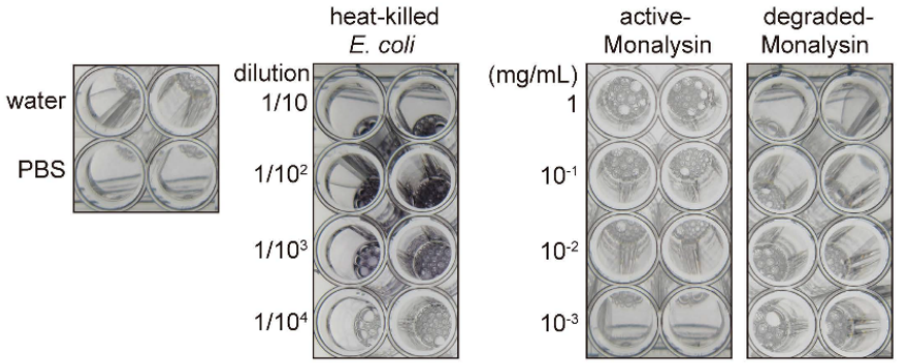

Figure 21. Contamination level of peptidoglycan in purified Monalysin.
0.001-1 mg/mL active-Monalysin, degraded Monalysin were incubated with Silkworm Larvae Plasma (SLP) reagent at 25°C for 30 min in a 96-well plate. Contamination level was monitored as blackness derived from melanin pigment which are produced in sample containing peptidoglycan. As a positive control, 10-10000 times dilution (1/10, $1/10^2$, $1/10^3$, $1/10^4$) of heat-killed *E. coli* prepared after overnight culture were also applied for same test.

Table

Table 1. Purification of pro-Monalysin

Fraction		Total protein (mg)	Total activity[a] (units)	Specific activity[b] (units/mg protein)	Purifi-cation (fold)	Yield (%)
I	Total lysate	3.5	3.1×10^3	8.7×10^2	1.0	100
II	25–50% (NH4)2SO4 ppt[c]	2.6	1.7×10^3	6.8×10^2	0.78	57
III	Anion exchange HPLC	2.3×10^{-1}	1.6×10^3	7.0×10^3	8.0	52
IV	0–50% (NH4)2SO4 ppt	6.0×10^{-2}	4.7×10^2	8.4×10^3	9.7	16
V	Gel filtration HPLC	2.0×10^{-2}	1.8×10^2	1.2×10^4	1.4	6

[a]Total activity was calculated as 1 unit corresponding to activity that yields 70% cell viability.
[b]Specific activity indicates total activity divided by total protein.
[c]ppt: precipitate.

References

[1] N. Vodovar *et al.*, "*Drosophila* host defense after oral infection by an entomopathogenic *Pseudomonas* species," *Proc. Natl. Acad. Sci. U. S. A.*, vol. 102, no. 32, pp. 11414-11419, 2005.

[2] G. Dieppois, O. Opota, J. Lalucat, & B. Lemaitre, (2015). *Pseudomonas entomophila*: a versatile bacterium with entomopathogenic properties. In *Pseudomonas*. Springer, pp. 25-49, 2015.

[3] S. Chakrabarti, P. Liehl, N. Buchon, and B. Lemaitre, "Infection-Induced Host Translational Blockage Inhibits Immune Responses and Epithelial Renewal in the *Drosophila* Gut," *Cell Host Microbe*, vol. 12, no. 1, pp. 60-70, 2012.

[4] O. Opota *et al.*, "Monalysin, a Novel ß-Pore-Forming Toxin from the *Drosophila* Pathogen *Pseudomonas entomophila*, Contributes to Host Intestinal Damage and Lethality," *PLoS Pathog.*, vol. 7, no. 9, pp. 1-13, 2011.

[5] I. Iacovache, F. G. van der Goot, and L. Pernot, "Pore formation: An ancient yet complex form of attack," *Biochim. Biophys. Acta*, vol. 1778, no. 7–8., pp. 1611-1623, 2008.

[6] M. Bischofberger, M. R. Gonzalez, and F. G. van der Goot, "Membrane injury by pore-forming proteins," *Curr. Opin. Cell Biol.*, vol. 21, no. 4., pp. 589-595, 2009.

[7] M. R. Gonzalez, M. Bischofberger, L. Pernot, F. G. Van Der Goot, and B. Frêche, "Bacterial pore-forming toxins: The (w)hole story?" *Cell Mol. Life Sci.*, vol. 65, no. 3. pp. 493-507, 2008.

[8] N. Buchon, N. A. Broderick, S. Chakrabarti, and B. Lemaitre, "Invasive and indigenous microbiota impact intestinal stem cell activity through multiple pathways in *Drosophila*," *Genes Dev.*, vol. 23, no. 19, pp. 2333-2344, 2009.

[9] I. Vallet-Gely, O. Opota, A. Boniface, A. Novikov, and B. Lemaitre, "A secondary metabolite acting as a signalling molecule controls *Pseudomonas entomophila* virulence," *Cell*

Microbiol., vol. 12, no. 11, pp. 1666-1679, 2010.

[10] J. L. Jurat-Fuentes and N. Crickmore, "Specificity determinants for Cry insecticidal proteins: Insights from their mode of action," *J. Invertebr. Pathol.*, vol. 142, pp. 5-10, 2017.

[11] A. Bravo *et al.*, "Evolution of *Bacillus thuringiensis* Cry toxins insecticidal activity," *Microb. Biotechnol.*, vol. 6, no. 1. pp. 17-26, 2013.

[12] F. Obata, S. Tanaka, S. Kashio, H. Tsujimura, R. Sato, and M. Miura, "Induction of rapid and selective cell necrosis in *Drosophila* using *Bacillus thuringiensis* Cry toxin and its silkworm receptor," *BMC Biol.*, vol. 13, no. 1, pp. 1-10, 2015.

[13] N. N. Jetha, M. Wiggin, and A. Marziali, "Forming an alpha-hemolysin nanopore for single-molecule analysis.," *Methods Mol. Biol.*, vol. 544, pp. 113-127, 2009.

[14] S. Nonaka *et al.*, "Molecular and Functional Analysis of Pore-Forming Toxin Monalysin From Entomopathogenic Bacterium *Pseudomonas entomophila*," *Front. Immunol.*, vol. 11, pp. 1-18, 2020.

[15] T. Kuraishi, O. Binggeli, O. Opota, N. Buchon, and B. Lemaitre, "Genetic evidence for a protective role of the peritrophic matrix against intestinal bacterial infection in *Drosophila melanogaster,*" *Proc. Natl. Acad. Sci. U. S. A.*, vol. 108, no. 38, pp. 15966-15971, 2011.

[16] P. Leone *et al.*, "X-ray and cryo-electron microscopy structures of Monalysin pore-forming toxin reveal multimerization of the pro-form," *J. Biol. Chem.*, vol. 290, no. 21, pp. 13191-13201, 2015.

[17] J. Manaka *et al.*, "Draper-mediated and phosphatidylserine-independent phagocytosis of apoptotic cells by *Drosophila* hemocytes/macrophages," *J. Biol. Chem.*, vol. 279, no. 46, pp. 48466-48476, 2004.

[18] N. Vodovar *et al.*, "Complete genome sequence of the entomopathogenic and metabolically versatile soil bacterium *Pseudomonas entomophila*," *Nat. Biotechnol.*, vol. 24, no. 6, pp. 673-679, 2006.

[19] J. S. Kim, S. Song, M. Lee, S. Lee, K. Lee, and N. C. Ha, "Crystal Structure of a Soluble Fragment of the Membrane Fusion Protein HlyD in a Type i Secretion System of Gram-Negative Bacteria," *Structure*, vol. 24, no. 3, pp. 477-485, 2016.

[20] I. D. Hay, M. J. Belousoff, and T. Lithgow, "Structural basis of type 2 secretion system engagement between the inner and outer bacterial membranes," *MBio*, vol. 8, no. 5, pp. 1-6, 2017.

[21] A. Bravo *et al.*, "Evolution of *Bacillus thuringiensis* Cry toxins insecticidal activity," *Microb. Biotechnol.*, vol. 6, no. 1, pp. 17-26, 2013.

[22] T. R. Graham and M. M. Kozlov, "Interplay of proteins and lipids in generating membrane curvature," *Curr. Opin. Cell Biol.*, vol. 22, no. 4, pp. 430-436, 2010.

[23] T. Asano and T. Nishiuchi, "Comparative analysis of phosphoprotein expression using 2D-DIGE.," *Methods Mol. Biol.*, vol. 744, pp. 225-233, 2011.

[24] H. Kenmoku, H. Ishikawa, M. Ote, T. Kuraishi, and S. Kurata, "A subset of neurons controls the permeability of the peritrophic matrix and midgut structure in *Drosophila* adults," *J. Exp. Biol.*, vol. 219, no. 15, pp. 2331-2339, 2016.

[25] K. Funakoshi, H. Suzuki, and S. Takeuchi, "Lipid bilayer formation by contacting monolayers in a microfluidic device for membrane protein analysis," *Anal. Chem.*, vol. 78, no. 24, pp. 8169-8174, 2006.

[26] T. Gutsmann, T. Heimburg, U. Keyser, K. R. Mahendran, and M. Winterhalter, "Protein reconstitution into freestanding planar lipid membranes for electrophysiological characterization," *Nat. Protoc.*, vol. 10, no. 1, pp. 188-198, 2015.

[27] T. Ando, N. Kodera, E. Takai, D. Maruyama, K. Saito, and A. Toda, "A high-speed atomic force microscope for studying biological macromolecules," *Proc. Natl. Acad. Sci. U. S. A.*, vol. 98, no. 22, pp. 12468-12472, 2001.

[28] T. Ando, T. Uchihashi, and S. Scheuring, "Filming biomolecular processes by high-speed

atomic force microscopy," *Chemical Reviews*, vol. 114, no. 6, pp. 3120-3188, 2014.

[29] N. Yilmaz, T. Yamada, P. Greimel, T. Uchihashi, T. Ando, and T. Kobayashi, "Real-time visualization of assembling of a sphingomyelin-specific toxin on planar lipid membranes," *Biophys. J.*, vol. 105, no. 6, pp. 1397-1405, 2013.

[30] C. Leung *et al.*, "Stepwise visualization of membrane pore formation by suilysin, a bacterial cholesterol-dependent cytolysin," *Elife*, vol. 3, pp. 1-17, 2014.

[31] T. Uchihashi, H. Watanabe, and N. Kodera, "Optimum substrates for imaging biological molecules with high-speed atomic force microscopy," in *Methods in Molecular Biology*, vol. 1814, Humana Press Inc., pp. 159-179, 2018.

Appendix

List of Appendix Figures and Figure Legends

Note:

- Electrophysiology study to monitor the pore formation of Monalysin was performed by Prof. Shoji Takeuchi from The University of Tokyo and Prof. Koki Kamiya from Kanagawa Institute of Industrial Science and Technology
- MALDI-TOF/TOF analysis was performed by Prof. Takumi Nishiuchi from Institute for Gene Research, Kanazawa University
- HS-AFM analysis, was performed together by me, Assoc. Prof. Takayuki Kuraishi and Prof. Noriyuki Kodera from WPI Nano Life Science Institute, Kanazawa University.

Appendix 1. Electrophysiology characterization of Monalysin as a pore-forming toxin

We performed functional analysis to confirm whether the endogenous Monalysin is a PFT and characterize its mode-of-action. This analysis was performed by our collaborator, Prof. Shoji Takeuchi from The University of Tokyo and Prof. Koki Kamiya from Kanagawa Institute of Industrial Science and Technology

We applied "on-chip lipid bilayer system" to examine the formation of pore on the lipid membrane. This system contains artificial planar bilayer lipid membrane (BLM) wells and parallel device with 16 separate channels (16-ch) to record ion current (Figure A. 1) [25]. First, the formation of Monalysin nanopores onto lipid bilayer were monitored and we found stepwise signals specific to nanopore-containing proteins in the solution which contained the active-Monalysin (Figure A. 1). A total of 723 stepwise signals for active-Monalysin and 35 stepwise signals for pro-Monalysin were observed for 30 min (Figure A. 2) suggesting that reconstitution of the trypsin-treated active-Monalysin into the lipid bilayer were more stronger and nanopores were formed within it.

Next, we examined the formation of active-Monalysin nanopores on lipid bilayers which composed of dioleoylphosphatidylcholine (DOPC) and dioleoylphosphatidylcholine, dioleoylphosphatidylserine, and dioleoylphosphatidylethanolamine (DOPC/DOPS/DOPE) with molar ratio of 7:2:1. The formation of the Monalysin nanopores was more occurrent on the DOPC lipid bilayer (723 stepwise signals) than the DOPC/DOPS/DOPE lipid bilayer (349 stepwise signals) (Figure A. 3 C). We obtained two amplitude peaks for the active-Monalysin-specific stepwise signals in each case for the DOPC lipid bilayer: 15 ± 1.9 pA, 17.3 ± 1.9 pA, and 25.5 ± 2.2 pA (mean ± S.D.), and for the DOPC/DOPS/DOPE lipid bilayer: 12.3 ± 1.8 pA, 18.1 ± 2.0 pA, and 26.1 ± 2.7 pA (mean ± S.D.) (Figure A. 3 A & B). We found that the amplitude peaks of the active-Monalysin signals were not significantly different between the DOPC and DOPC/DOPS/DOPE bilayers. Based on the method described in Gutsmann et al., we estimated the diameters of the active-Monalysin nanopores from the

amplitude of the active-Monalysin signals and buffer conductance [26]. Using the amplitude peaks, in case of the DOPC lipid bilayer, the estimated diameters of the active-Monalysin were 0.74 ± 0.30 nm, 0.91 ± 0.30 nm, and 1.10 ± 0.32 nm (mean ± S.D.), and 0.77 ± 0.30 nm, and in case of the DOPC/DOPS/DOPE lipid bilayer were 0.77 ± 0.29 nm, 0.93 ± 0.31 nm, and 1.12 ± 0.36 nm (mean ± S.D.). To sum up, Monalysin preferentially insert itself within a lipid bilayer with high ratio of PC, and forms nanopores with diameters to be around 0.7-1 nm in any lipid composition.

Appendix 2. Atomic Force Microscope Analysis for the Structure of Monalysin in Solution

Gel filtration chromatography of endogenous Monalysin indicates that Monalysin forms a stable pore-forming complex prior to its activation and membrane interaction, in line with the previous report [16]. Yet, according to the gel filtration analysis, the molecular weight of an endogenous Monalysin complex seems to be slightly smaller than that of a previous 18-mer model of Monalysin. This estimate is in line with the data from an MALDI-TOFMS analysis. We found a possible molecular ion peak of active-Monalysin multimers with m/z was 217932.23. This value was very close to the molecular weight of an 8-mer active-complex expected from the amino acid sequences, 213160.4 Da (Figure A. 4). The knowledge about the structure and dynamic nature of endogenous Monalysin in solution and lipid membrane is very important to understand its molecular function in detail, and use to study the mechanism of innate immunity in flies, as well as to develop biological nanopores and biological insecticides. Thus, we applied HS-AFM that able to monitor the real-time dynamic of macromolecule at nanometer resolutions, which other methods are unable to perform it [27], [28]. Recent studies indicate that this method is able to reveal the dynamic structures of pore-forming proteins [28]–[30].

First, pro-Monalysin diluted in the PBS buffer dropped on a mica surface was observed. Figure A. 5 shows the experimental setup. We observed a similar height of molecules on the mica surface as indicated in Figure A. 6. We also observed trefoil-shaped molecules at smaller scan sizes (Figure A. 6). Importantly, the molecule corresponding to each leaf of the trefoil dissociated from, and re-bound to, a trefoil-shaped molecule (Figure A. 7, 9.75, and 10.25 s), suggesting that one particle in the trefoil-shaped molecule is the minimum unit of pro-Monalysin. Note that, in the solution, sometimes pro-Monalysin forms a trimer of the minimum unit. Hereafter, this minimum unit of pro-Monalysin is referred as pro-form. The pro-form height was 14.0 ± 0.9 nm (mean ± S.D) as indicated in Figure A. 9 A and B. The center-to-center distance between the adjacent pro-forms in the trefoil-shaped molecule was 11.3 ± 1.7 nm (Figure A. 9 C) suggesting that this distance corresponds to the maximal diameter

of the pro-form, which is slightly smaller compared to that of recombinant Monalysin with the diameter around 14 nm, as previously reported [16]. The existence of the reported pore structure on the center of the pro-form was unable to be confirmed due to the movement speed of the pro-form was faster than that of AFM scanning speed.

Then, we monitored the structure of active-Monalysin in the PBS buffer on a mica surface and found that no molecules with trefoil shape were detected (Figure A. 8 and Figure A. 10). The remarkable difference was the height of the active-form was 5.1 ± 0.3 nm (Figure A. 10 B and C), which is less than half of the pro-form. This finding supports the idea that pro-Monalysin is made up of two double-stacked disk-like oligomers that split into two disk-shaped oligomers after proteolytic cleavage [16]. This results also suggest that active-form of Monalysin can be observed.

Next, to allow us to image high spatial resolution of the molecular feature of the active-Monalysin, we used a low salt buffer (30 mM NaCl, 10 mM Sodium phosphate, pH7.0) as an observation buffer which induced strong immobilization of Monalysin oligomers on the mica surface. Using this buffer we clearly visualized oligomers with a central pore even at wider scan sizes (Figure A. 8). We found that the height of active-Monalysin was 5.3 ± 0.3 nm (mean ± S.D.) (Figure A. 9 D and E) which was similar to that found under the PBS buffer. Figure A. 9D indicates that the aperture diameter of the active-Monalysin was around 3 nm, similar to that of reported in the previous study [16]. The center-to-center distance between the adjacent active-forms was 11.4 ± 0.9 nm (Figure A. 9F), suggesting that the maximal diameter of the active-form is identical to that of the pro-form. This result indicates that no significant alteration in the outer diameters of Monalysin after protease activation, in line with the previous report [16]. Interestingly, at a smaller scan size, it can be observed that the active-Monalysin had eight sub-units and formed a disk-shaped octamer (Figure A. 11). However, the previous report suggests that the crystalline structure of recombinant pro-Monalysin is nonameric (9-mer) [16].

Next, we visualized that after trypsin treatment in the PBS buffer, pro-Monalysin molecules with a height of ~14 nm were transformed into active-Monalysin with a height of ~5 nm over time which depend on the trypsin-concentration (Figure A. 12). Interestingly, even in the absence of trypsin treatment, we found that stronger tapping forces also induced the conversion of the pro-Monalysin with a height of ~14 nm to the active-Monalysin. However, this conversion was depended on the tapping force strength (Figure A. 13). This height change for almost all the pro-form molecules can be observed 60 s after Asp/A0 at 0.5 were applied (the average tapping force is estimated to be 53 ± 17 pN). However, no height change were observed when we used Asp/A0 of more than 0.8 with average tapping force of <37 ± 17 pN, even the force were applied after 60 s. These findings clearly suggest that proteolytic cleavage activity of trypsin, not the mechanical perturbations, is responsible for the change in pro-Monalysin height. Thus, the data in Figure A. 12 are direct evidence that trypsin treatment effectively cleaves a portion of pro-Monalysin and dissociates the doubly stacked disks to produce the active-forms. The active-forms can endure a tapping force of ~50 pN on average (Figure A. 13 D,E). Furthermore, the pro-form height alternated from 14 to 5 nm only when the molecules were firmly immobilized on the mica surface under the low salt buffer (Figure A. 14). Notably, the pro-Monalysin not activated by trypsin treatment, was highly immobilized on the mica surface, forming a disk-shaped octamer with a central pore (Figure A. 14B). This result is in line with the previous report [16] which suggest that the central pore is already established in the doubly stacked disks of pro-Monalysin in solution.

Appendix 3. Real-Time Dynamics of Monalysin Insertion Into a Lipid Bilayer

Next, the insertion events of the active-Monalysin into a lipid membrane were visualized (Figure A. 15). On the surface of polydimethylsiloxane (PDMS), a lipid membrane was formed from a mixture of phospholipids from DOPC/DOPS/biotin-cap-DOPE [31]. Then we added the active-Monalysin into the observation buffer to be monitored. HS-AFM showed that the active-Monalysin was inserted into the lipid membrane without significant structural change (Figure A. 15). The sub-unit stoichiometry was directly resolved to be 8-mer at smaller scan sizes (Figure A. 15D). These findings indicate that endogenous pro-Monalysin is a 16-mer complex that is divided into 8-mer active complexes by protease and then incorporated into the lipid membrane as they are. Interestingly, Monalysin was shown to be preferentially inserted into the lipid membrane's edge (Figure A. 15E) implying that it prefers to be inserted in highly curved parts of the membrane.

Appendix Figures and Figure legends

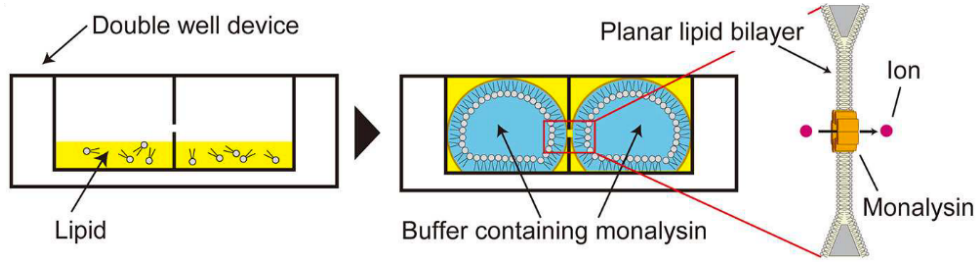

Figure A. 1. Experimental design to monitor the pore formation of Monalysin.
The lipid was supplied into the double well device, then a buffer containing Monalysin was added to a planar bilayer lipid membrane which was formed based on the droplet contact method, and ion current signals were recorded to monitor pore formation.

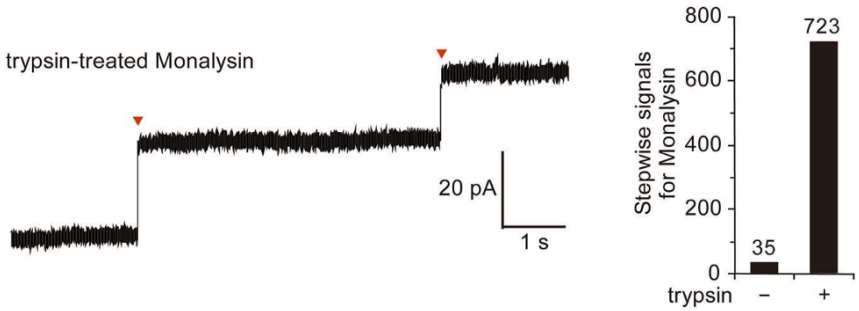

Figure A. 2. Typical current signal of the Monalysin.
The Monalysin was digested by trypsin. Red triangles indicate the detections of a single Monalysin nanopore within the BLM. Monalysin signals were monitored for 30 min with applied potential of +100 mV using a 16-ch device (Figure A. 1). Total stepwise signals of Monalysin, with or without trypsin treatment, on the DOPC lipid bilayer were displayed (Right).

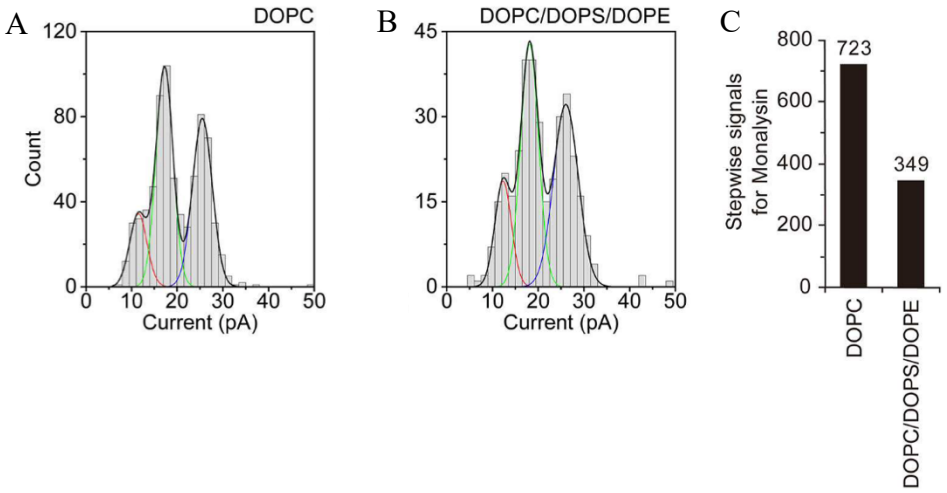

Figure A. 3. Current-amplitude histogram of the Monalysin onto lipid bilayers.
The lipid bilayers were composed of DOPC and DOPC/DOPS/DOPE (mol ratio of 7:2:1). Total signals of Monalysin on the DOPC and DOPC/DOPS/DOPE lipid bilayer were displayed (Right). Monalysin signals were observed using a 16-ch device for 30 min. The curve represents a multipeak Gaussian fitting ($P < 0.05$, F-test, respectively): the red, green and blue curves indicate the first, second and third Gaussian peak, respectively, and the black curves indicate the sum of the three Gaussian curves.

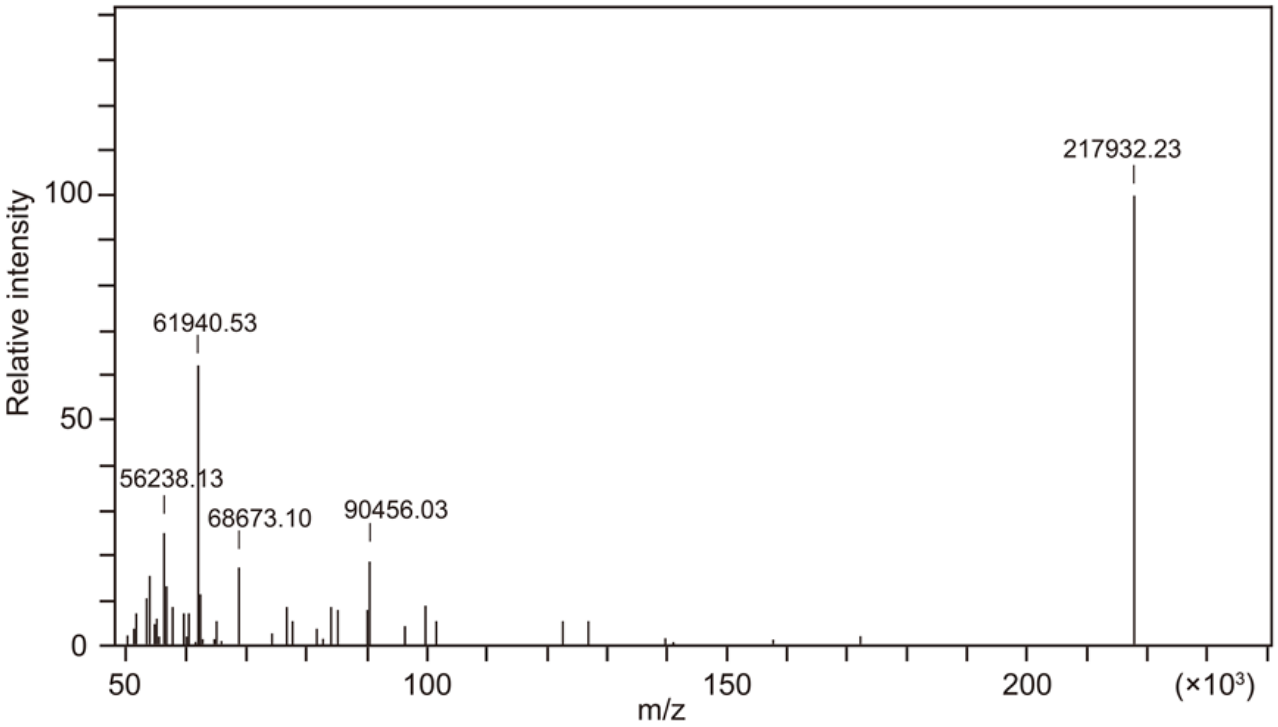

Figure A. 4. MALDI-TOF/TOF analysis of active-Monalysin.

MALDI-TOF/TOF analysis on active-Monalysin solution, which had been obtained from the short trypsin treatment of pro-Monalysin. The mass spectrum shows integrated data via analysis software. The highest signal with m/z was 217932.23, indicates a possible molecular ion peak of active-Monalysin multimers.

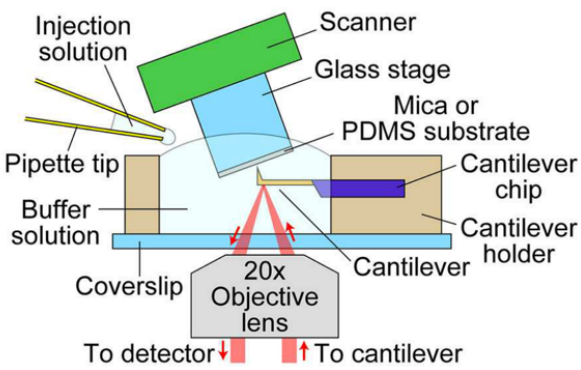

Figure A. 5. Experimental design for AFM analysis.
Samples were absorbed into a substrate surface and imaged by a probe-tip attached at the end of a cantilever. In some experiments, the injection solution was added to the buffer solution during AFM imaging.

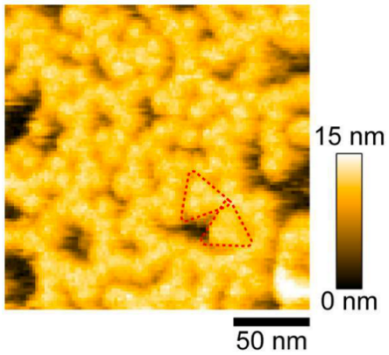

Figure A. 6 A wide-area image of pro-Monalysin.
Red dashed-lines indicate the typical trefoil-shaped molecules. The scanning area was 200 × 200 nm^2 with 100 × 100 pixels, and the imaging rate was 330 ms/frame.

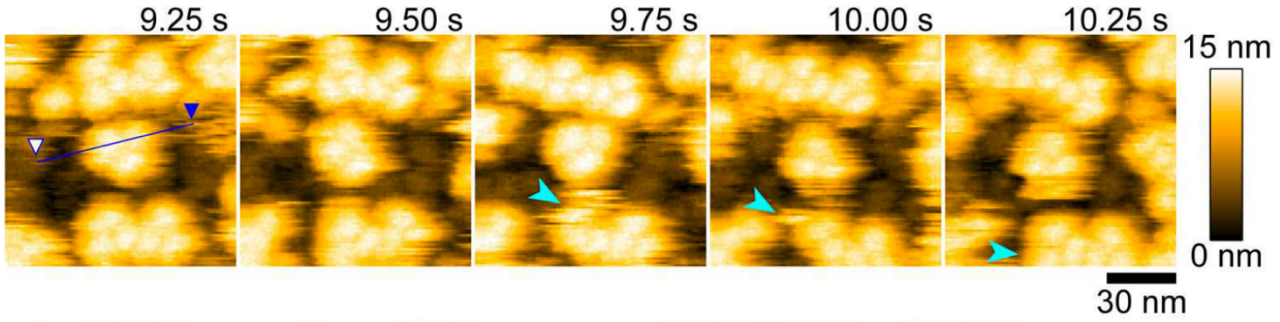

Figure A. 7. Successive AFM images of pro-Monalysin.
The light blue arrowhead shows that a pro-form detaches from, and binds to, a trefoil-shaped molecule. The scanning area was 100 × 100 nm^2 with 100 × 100 pixels and the imaging rate was 250 ms/frame.

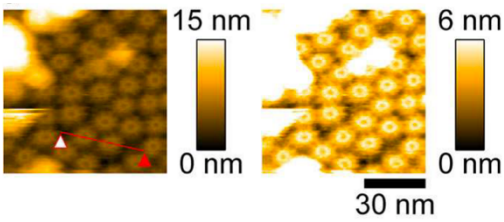

Figure A. 8. A wide-area image of active-Monalysin.
Two different height scale images are shown. Bright spots are some adsorbed debris. The scanning area was 80 × 80 nm^2 with 160 × 160 pixels and the imaging rate was 330 ms/frame.

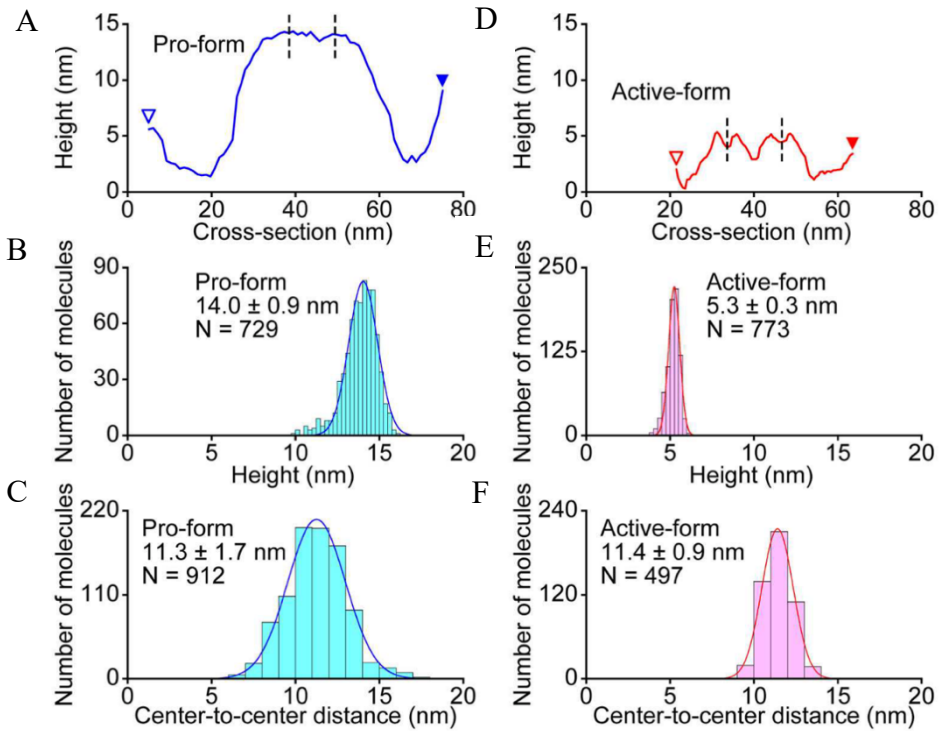

Figure A. 9. A cross-section analysis of pro-Monalysin and active-Monalysin.
A cross-section analysis of pro-Monalysin (A) and active-Monalysin (B) which were drawn from the images in Figure A.6 & A.8 for pro-Monalysin and active-Monalysin, respectively. Each dashed line indicates the center position of a molecule used in the analysis of C,F. (B,E) Height distributions of pro- and active-Monalysin. (C,F) Center-to-center distance distributions of pro- and active-Monalysin. All distributions were fitted by single-Gaussian curve.

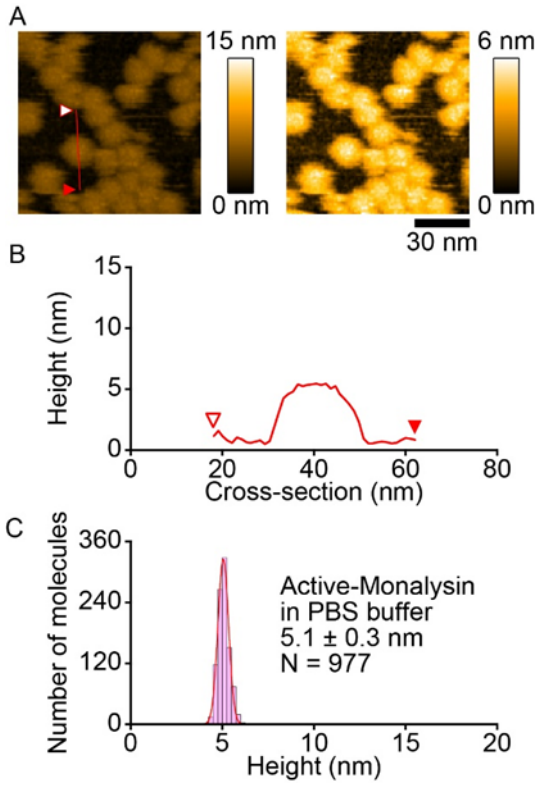

Figure A. 10. Molecular features of active-Monalysin on mica surface in PBS buffer.
(A) AFM images of active-Monalysin in a PBS buffer. Two different height scale images are shown. The scanning area was 100 × 100 nm^2 with 100 × 100 pixels and the imaging rate was 250 ms/frame. **(B)** Cross-section analysis. The section is from the red line drawn on the images in A. **(C)** Height distributions of active-Monalysin observed in PBS buffer. The distribution was fitted by a single-Gaussian curve.

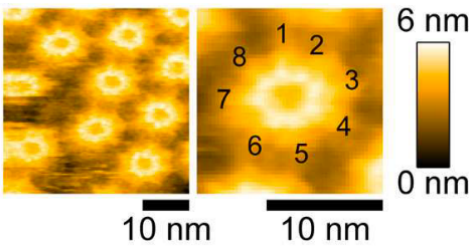

Figure A. 11. Small-area image of active-Monalysin.
The scanning area was 40 × 40 nm^2 with 120 × 120 pixels, and the imaging rate was 150 ms/frame.
The right image is an averaged image using four successive images.

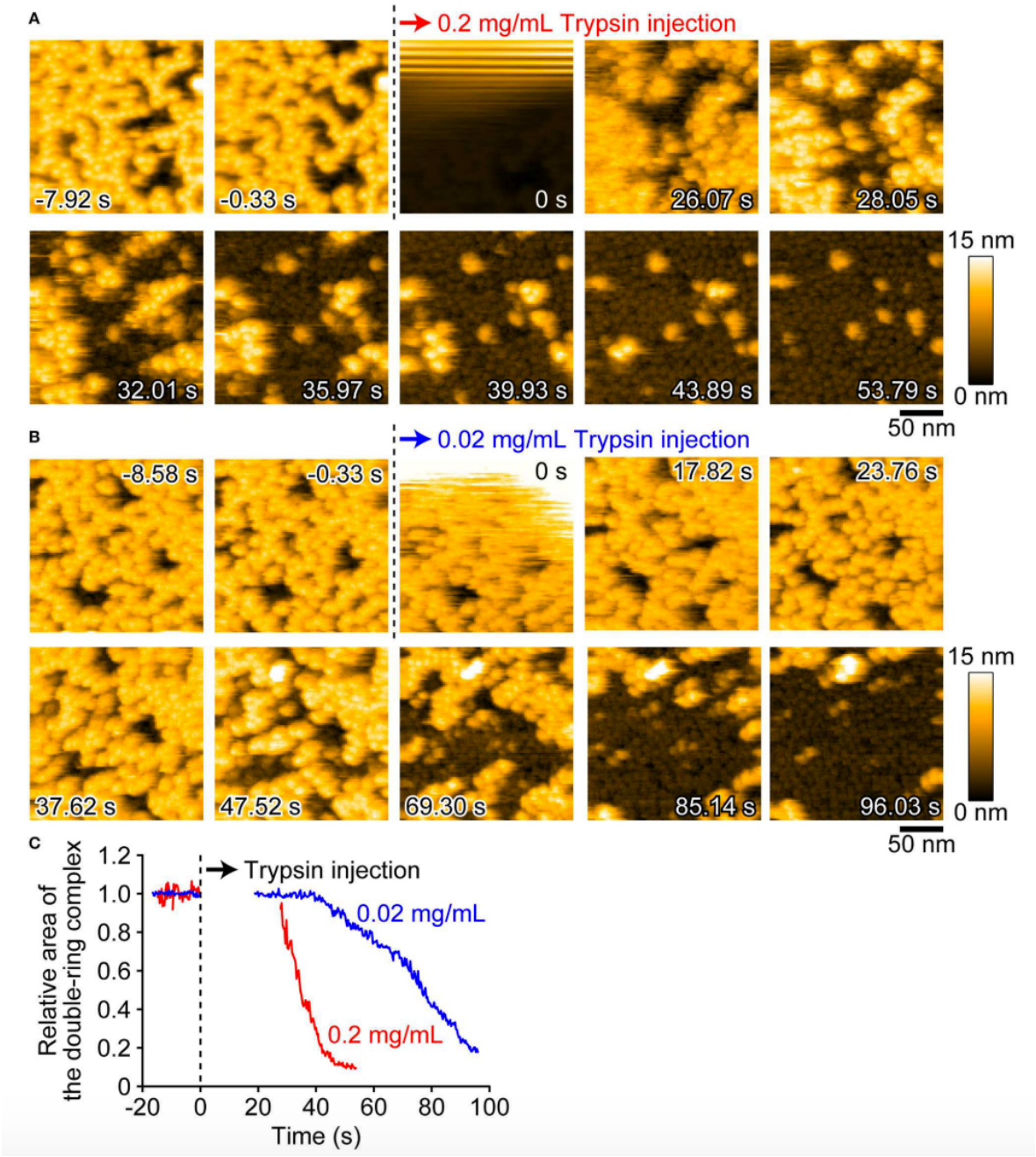

Figure A. 12. AFM images showing the height conversion of pro-Monalysin upon trypsin treatment. (A,B) Successive AFM images before and after trypsin injection. The scanning area was 200 × 200 nm^2 with 100 × 100 pixels, and the imaging rate was 330 ms/frame.
At 0 s, in the observation buffer, a drop of trypsin solution was injected at the final concentrations of trypsin in the observation buffer were 0.2 mg/mL for A and 0.02 mg/mL for B, respectively. The height change was gradually observed following injection. (C) The time course of the relative area of the double-ring complex of pro-Monalysin before and after trypsin injection. The average coverage area before trypsin injection is set to 1. The time course after injection is missed for 20-30 seconds due to the AFM images were disrupted at this time, making area measurements cannot be carried out.

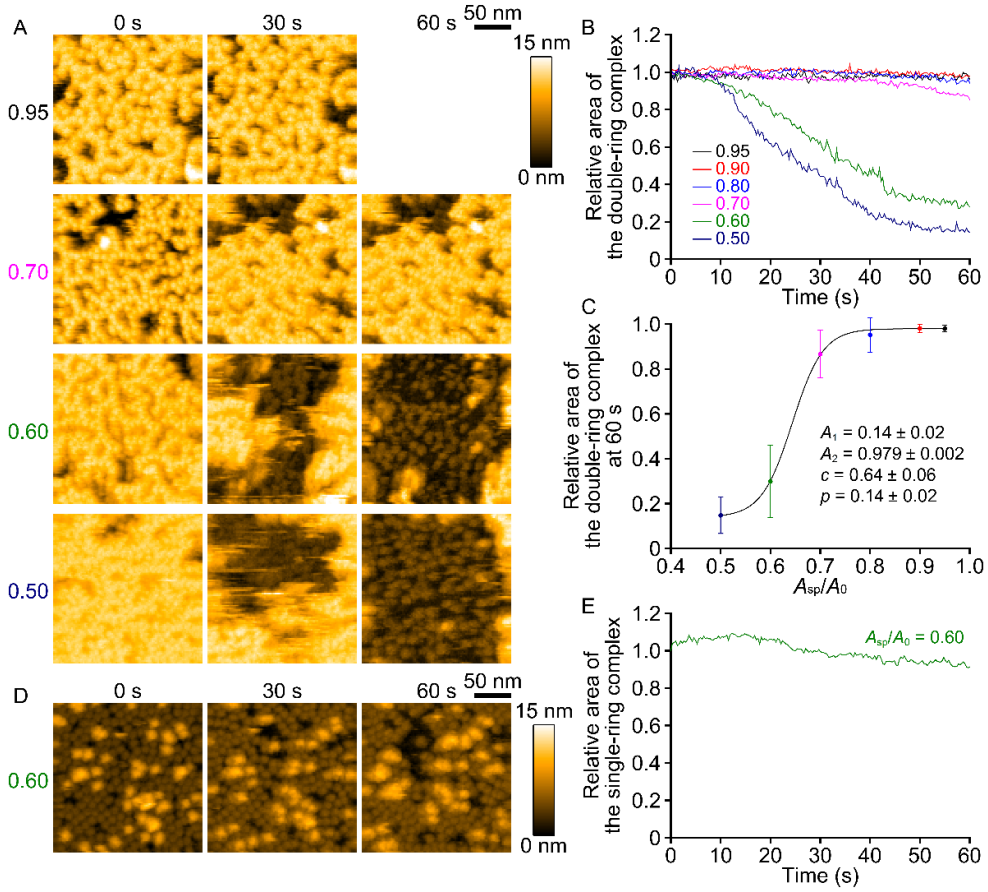

Figure A. 13. AFM imaging of Monalysin under different tapping forces.

(A) AFM images of pro-Monalysin under the different A_{sp}/A_0 conditions. From the top, A_{sp}/A_0 was set to 0.95, 0.70, 0.60 and 0.50, respectively. The scanning area was 200 × 200 nm^2 with 100 × 100 pixels and the imaging rate was 330 ms/frame. **(B)** The time course of the relative area of double-ring complex of pro-Monalysin after setting of A_{sp}/A_0. The line colors correspond to the settings of A_{sp}/A_0. The coverage area of the first image is set to 1. Each time course is an average one calculated from more than three different measurements. Note that the area of double-ring complex of pro-Monalysin was calculated by counting the pixels whose height was more than 8 nm. **(C)** The relative area of the double-ring complex at 60 s as a function of A_{sp}/A_0. Each data point was calculated from the same measurements described above. The data points were fitted by the dose-response relationship curve as follows.

$$y = A_1 + \frac{A_2 - A_1}{1 + 10^{p(c-x)}}$$

The fitting parameters are shown in the graph. **(D)** AFM image of active-Monalysin under the A_{sp}/A_0 of 0.6. The scanning area was 200 × 200 nm^2 with 100 × 100 pixels, and the imaging rate was 330 ms/frame. **(E)** The time course of the relative area of the single-ring complex of active-Monalysin after setting of A_{sp}/A_0. The coverage area of the first image is set to 1. Note that the area of the single-ring complex was calculated by counting the pixels whose height was in a range from 4 to 8 nm, meaning that the measurement errors from the adsorbed debris were minimized.

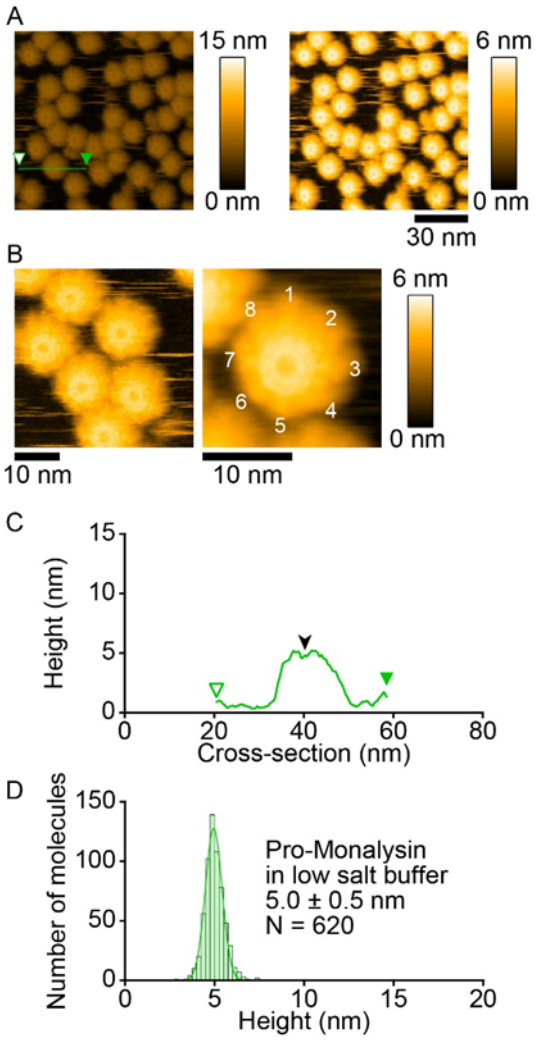

Figure A. 14. Molecular features of pro-Monalysin on mica surface in a low salt buffer (30 mM NaCl, 10 mM Sodium phosphate, pH7.0).
(A) A wide-area image of pro-Monalysin in the low salt buffer. Images of two different height scales are shown. The scanning area was 100 × 100 nm^2 with 300 × 300 pixels, and the imaging rate was 1 s/frame. **(B)** Small-area image of pro-Monalysin in the low salt buffer. The scanning area was 40 × 40 nm^2 with 200 × 200 pixels, and the imaging rate was 0.5 s/frame. **(C)** Cross-section analysis. The section is from the green line drawn on the images in A. The black arrowhead indicates the central pore. **(D)** Height distributions of pro-Monalysin observed in the low salt buffer. The distribution was fitted by a single-Gaussian curve.

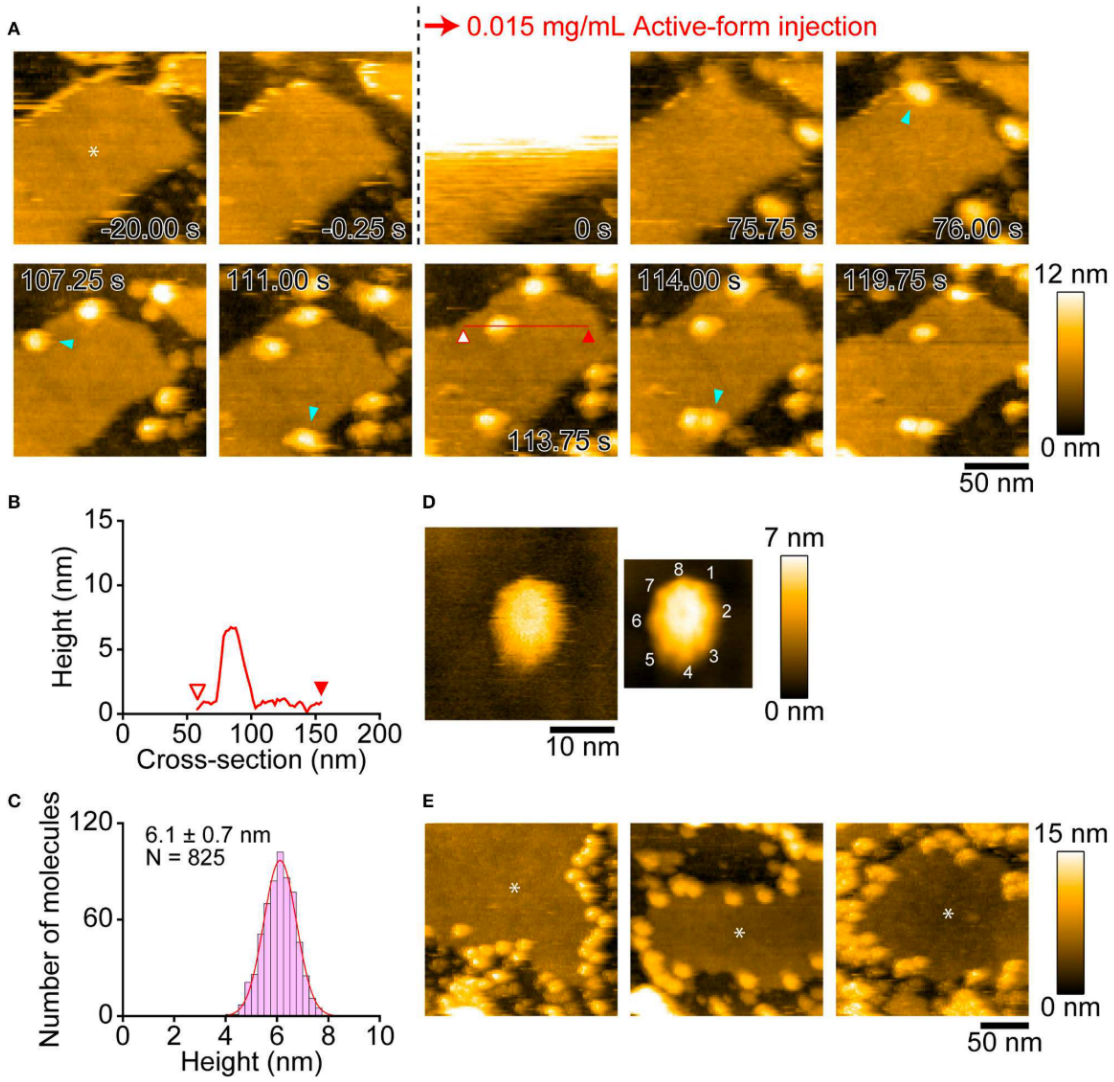

Figure A. 15. AFM images showing insertion of active-Monalysin onto lipid membrane formed on the PDMS surface.

(A) Successive AFM images before and after active-Monalysin injection. Dark area represents the PDMS surface, while slightly bright area represents the lipid membrane surface (see the asterisk in the first image). The scanning area was 150 × 150 nm^2 with 80 × 80 pixels, and the imaging rate was 250 ms/frame. At 0 s, a drop of active-Monalysin solution was injected in the observation buffer. The final concentrations of active-Monalysin in the observation buffer were 0.015 mg/mL. After injection, the active-Monalysin were gradually inserted on the lipid bilayer (see the light blue arrowheads). (B) A cross-section analysis of active-Monalysin inserted in the lipid bilayer. The section is from the red line drawn on the image in A. (C) Height distributions of active-Monalysin inserted in the lipid bilayer. The distribution was fitted by single-Gaussian curve. (D) Small-area image of active-Monalysin inserted in the lipid bilayer. The scanning area was 30 × 30 nm^2 with 150 × 150 pixels, and the imaging rate was 330 ms/frame. The right image is an averaged image using 20 successive images. (E) AFM image gallery showing that the active-Monalysin are preferentially inserted into the edge of lipid bilayer. Asterisk marks represent the lipid bilayer areas. The scanning area was 200 × 200 nm^2 with 100 × 100 pixels, and the imaging rate was 330 ms/frame.

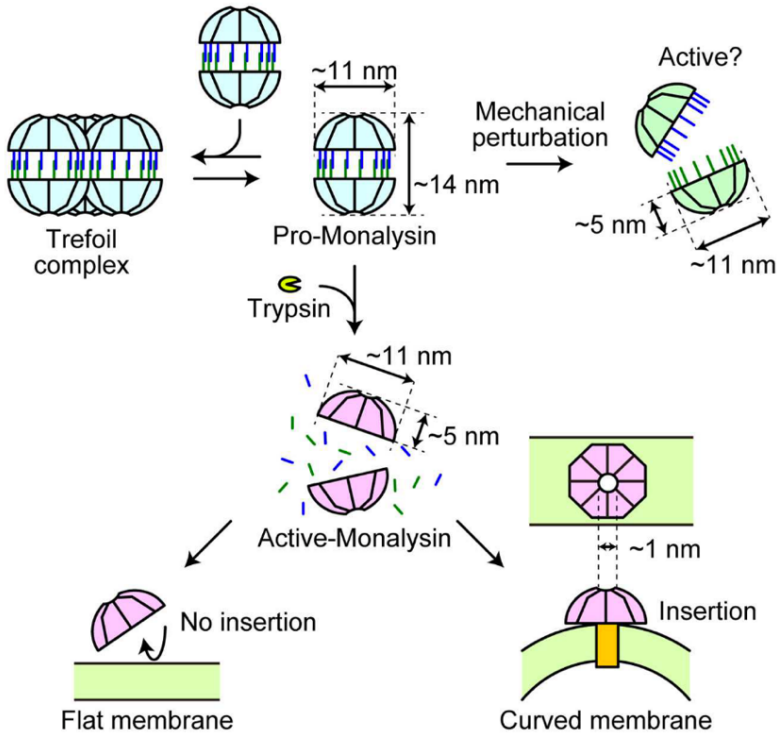

Figure A. 16. A model of Monalysin activation for pore formation.
Endogenous Monalysin forms a 16-mer complex in the PBS buffer and sometimes forms a trefoil-shaped structure consisting of trimer complex when its concentration is high enough. The double-stacked disk-like 16-mer complex dissociates into two disk-shaped 8-mer complexes after trypsin treatment or mechanical perturbation. The active-Monalysin 8-mer complex then preferentially integrates itself into the curved lipid membrane, forming nanopores (pore size = 1 nm).